



CERN-EP-2025-185
 LHCb-PAPER-2025-027
 September 3, 2025

Amplitude analysis of $B^0 \rightarrow \eta_c(1S)K^+\pi^-$ decays

LHCb collaboration[†]

Abstract

An amplitude analysis of the $B^0 \rightarrow \eta_c(1S)K^+\pi^-$ decays with $\eta_c(1S) \rightarrow p\bar{p}$ is performed using a sample corresponding to an integrated luminosity of 9 fb^{-1} of $p\bar{p}$ collision data collected by the LHCb detector at centre-of-mass energies of $\sqrt{s} = 7, 8$ and 13 TeV . The data are described with a model including only intermediate contributions from known K^{*0} resonances. Evidence for an exotic resonance in the $\eta_c(1S)\pi^-$ system, reported in a previous analysis of this decay channel, is not confirmed. The inclusive branching fraction of the $B^0 \rightarrow \eta_c(1S)K^+\pi^-$ decays is measured to be

$$\mathcal{B}(B^0 \rightarrow \eta_c(1S)K^+\pi^-) = (5.82 \pm 0.20 \pm 0.23 \pm 0.55) \times 10^{-4},$$

where the first uncertainty is statistical, the second systematic, and the third arises from the limited knowledge of external branching fractions.

Submitted to Eur. Phys. J. C

© 2025 CERN for the benefit of the LHCb collaboration. [CC BY 4.0 licence](#).

[†]Authors are listed at the end of this paper.

1 Introduction

Since the formulation of the quark model, hadronic states beyond the conventional $q\bar{q}$ mesons and qqq baryons have been proposed. Models based on quantum chromodynamics predict the existence of various nonconventional hadrons, composed of different combinations of quarks and gluons, including glueballs, molecular states and tightly bound states, such as pentaquarks ($qqqq\bar{q}$) and tetraquarks ($qq\bar{q}\bar{q}$) [1, 2]. In the early 2000s, a hadron with unexpected properties, the $\chi_{c1}(3872)$ meson, was observed [3], followed shortly by the discovery of many other charmonium-like and bottomonium-like states [4–7]. In some cases the properties of these states, including their electric charge, are inconsistent with predictions from conventional $q\bar{q}$ models. Various interpretations have been proposed regarding their nature, binding and production mechanisms, and internal structure [8–13]. To advance the understanding of these exotic hadrons, it is essential to investigate alternative production mechanisms and decay modes of previously observed unconventional states, while also searching for new candidates.

The BESIII collaboration observed in the $J/\psi\pi^+\pi^-$ final state a resonance whose minimal composition requires the presence of two quarks and two antiquarks [14], denoted $T_{c\bar{c}1}(3900)^-$, later confirmed also by the Belle [15] and CLEO collaborations [16]. This state has been interpreted as a hadrocharmonium state with J/ψ embedded in excited light-quark matter [17], implying a partner state where the J/ψ is replaced by the $\eta_c(1S)$. Such a state would correspond to an isovector resonance decaying to $\eta_c(1S)\pi^-$ with similar structure and quantum numbers.¹ This interpretation is further supported by heavy-quark spin symmetry [17], lattice QCD [18], and diquark models [9], which all foresee such a decay channel.

Evidence of a state decaying to $\eta_c\pi^-$, named $T_{c\bar{c}}(4100)^-$, has been found in the previous analysis of $B^0 \rightarrow \eta_c K^+\pi^-$ decays by the LHCb collaboration [19] using a data sample of pp collisions corresponding to an integrated luminosity of 4.7 fb^{-1} , collected in 2011, 2012 and 2016 at centre-of-mass energies of $\sqrt{s} = 7, 8,$ and 13 TeV , respectively.² The mass and natural width of this resonance are measured to be $4096 \pm 20^{+18}_{-22} \text{ MeV}$ and $152 \pm 58^{+60}_{-35} \text{ MeV}$, respectively.³ Since this would make the state significantly more massive than the $T_{c\bar{c}1}(3900)^-$ state, it cannot be its expected partner. Following the evidence reported by the LHCb collaboration for the $T_{c\bar{c}}(4100)^-$ charmonium-like candidate, several theoretical studies have been conducted to investigate its nature. The authors of Ref. [20] calculated the mass, width, and coupling of this resonance, treating it as a scalar four-quark system with a diquark–antidiquark structure. Other studies found the $T_{c\bar{c}}(4100)^-$ state to be compatible with the tetraquark hypothesis favouring the quantum number $J^{PC} = 0^{++}$ based on the measured width [21]. The study reported in Ref. [22] suggests that the state can be described as hadrocharmonium, where the η_c charmonium core is embedded in an S-wave configuration inside an excited light-quark state with the quantum numbers of a pion, $I^G(J^P) = 1^-(0^-)$. It further proposes that the mass difference between the $T_{c\bar{c}1}(4200)^-$, observed in the $J/\psi K^+\pi^-$ final state [23, 24], and $T_{c\bar{c}}(4100)^-$ states should be similar to that between the J/ψ and η_c mesons, and that the partial widths of their dominant decays to $J/\psi\pi^-$ and $\eta_c\pi^-$, respectively, should be the same. There are also studies [25] proposing that $T_{c\bar{c}}(4100)^-$ is the charge-conjugate state of the $T_{c\bar{c}}(4050)^+$

¹The simplified notation η_c is used to refer to the $\eta_c(1S)$ meson.

²The inclusion of charge-conjugate processes is implied throughout.

³Natural units with $\hbar = c = 1$ are used throughout.

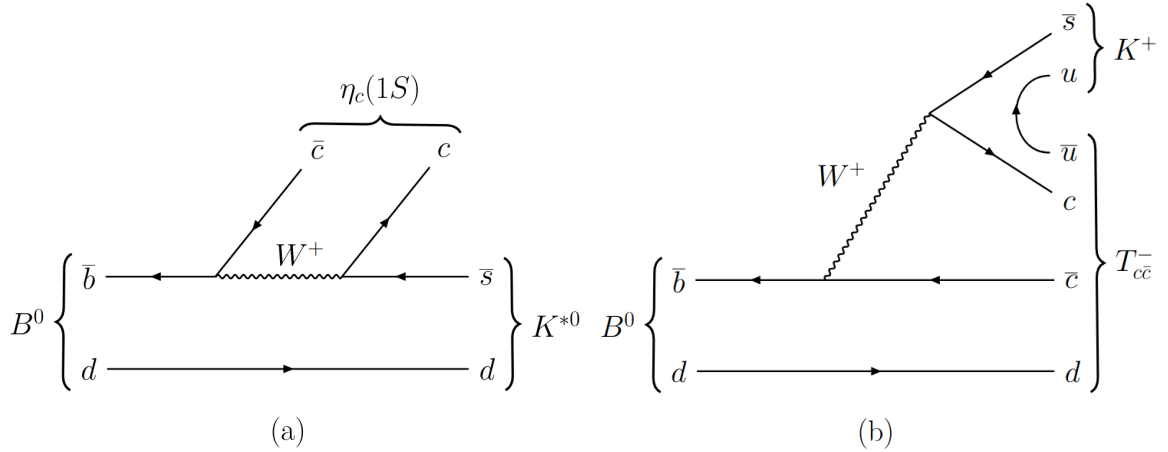


Figure 1: Feynman diagrams for the (a) $B^0 \rightarrow \eta_c(1S) K^{*0}$ and (b) $B^0 \rightarrow T_{c\bar{c}}(4100)^- K^+$ decay modes.

state observed by the Belle collaboration in the $\chi_{c1}\pi^+$ final state [26]. Finally, it has been suggested that the observed structure could be a kinematic effect arising from an S-wave $D^*\bar{D}^*$ pair rescattering with $I^G(J^{PC}) = 1^-(0^{++})$ or a resonance produced by the P-wave $D^*\bar{D}^*$ interaction [27].

This letter reports an updated study of the $B^0 \rightarrow \eta_c K^+ \pi^-$ decay with a dataset approximately twice the size of the one used in Ref. [19] which enables a more precise evaluation of the presence of exotic contributions in this decay, as well as a more accurate determination of their properties. The $B^0 \rightarrow \eta_c K^+ \pi^-$ decay is expected to be dominated by the $K^*(892)^0 \rightarrow K^+ \pi^-$ resonance, with some contributions from other $K^{*0} \rightarrow K^+ \pi^-$ resonances. The decay could also proceed through exotic intermediate states, which could result in resonant structures in the $\eta_c \pi^-$ system. The Feynman diagrams of the $B^0 \rightarrow \eta_c K^+ \pi^-$ decay are shown in Fig. 1. The $B^0 \rightarrow \eta_c K^+ \pi^-$ decay is studied by reconstructing the η_c meson through its $p\bar{p}$ decay mode rather than the dominant mesonic modes. This choice avoids the need to distinguish between kaons and pions originating from B^0 decay, reducing associated systematic uncertainties [28]. The $B^0 \rightarrow \eta_c K^+ \pi^-$ decay involves only pseudoscalar mesons in the initial and final states and it is therefore fully described by two independent kinematic variables. This allows for a Dalitz plot (DP) [29] analysis, which provides a complete characterisation of the decay dynamics. The absolute branching fraction of the $B^0 \rightarrow \eta_c K^+ \pi^-$ decay is also measured, using the $B^0 \rightarrow J/\psi K^+ \pi^-$ decay as normalisation channel. The data sample corresponds to an integrated luminosity of 9 fb^{-1} of pp collision data collected by the LHCb detector at centre-of-mass energies of $\sqrt{s} = 7, 8,$ and 13 TeV in 2011, 2012 and 2015–2018, respectively. Data collected in 2011 and 2012 are referred to as Run 1 data, while data collected in 2015–2018 are referred to as Run 2 data.

2 Detector and simulation

The LHCb detector [30, 31] is a single-arm forward spectrometer covering the pseudorapidity range $2 < \eta < 5$, designed for the study of particles containing b or c quarks. The detector used to collect the data analysed in this paper includes a high-

precision tracking system consisting of a silicon-strip vertex detector surrounding the pp interaction region [32], a large-area silicon-strip detector located upstream of a dipole magnet with a bending power of about 4 T m, and three stations of silicon-strip detectors and straw drift tubes [33, 34] placed downstream of the magnet. The tracking system provides a measurement of the momentum, p , of charged particles with a relative uncertainty that varies from 0.5% at low momentum to 1.0% at 200 GeV. The minimum distance of a track to a primary pp collision vertex (PV), the impact parameter (IP), is measured with a resolution of $(15 + 29/p_T)$ μm , where p_T is the component of the momentum transverse to the beam, in GeV. Different types of charged hadrons are distinguished using information from two ring-imaging Cherenkov detectors [35]. Photons, electrons, and hadrons are identified by a calorimeter system consisting of scintillating-pad and preshower detectors, an electromagnetic and a hadronic calorimeter. Muons are identified by a system composed of alternating layers of iron and multiwire proportional chambers [36]. The online event selection is performed by a trigger system [37], which consists of a hardware stage, based on information from the calorimeter and muon systems, followed by a software stage, which applies a full event reconstruction.

At the hardware trigger stage, events are required to have a muon with high p_T or a hadron, photon or electron with high transverse energy in the calorimeters. For hadrons, the transverse energy threshold is 3.5 GeV. The software trigger requires a two-, three- or four-track secondary vertex with a significant displacement from any primary pp interaction vertex. At least one charged particle must have a transverse momentum $p_T > 1.6$ GeV and be inconsistent with originating from any PV. A multivariate algorithm [38, 39] is used for the identification of secondary vertices consistent with the decay of a b hadron.

Simulated events are used to develop the selection requirements, validate fit models, and to evaluate the efficiencies needed for the inclusive branching fraction measurement and the amplitude analysis. In the simulation, pp collisions are generated using PYTHIA [40] with a specific LHCb configuration [41]. Decays of unstable particles are described by EVTGEN [42], in which final-state radiation is generated using PHOTOS [43]. The interaction of the generated particles with the detector, and its response, are implemented using the GEANT4 toolkit [44] as described in Ref. [45]. The underlying pp interaction is reused multiple times, each with an independently generated signal decay [46].

3 Selection of $B^0 \rightarrow p\bar{p}K^+\pi^-$ candidates

Candidate B^0 mesons are reconstructed in the $B^0 \rightarrow p\bar{p}K^+\pi^-$ decay over the full $m_{p\bar{p}}$ range. The signal channel $B^0 \rightarrow \eta_c K^+\pi^-$ and the normalisation channel $B^0 \rightarrow J/\psi K^+\pi^-$ are obtained by requiring $m_{p\bar{p}}$ to lie within their respective charmonium-resonance regions, 2908–3058 MeV for the η_c meson and 3072–3122 MeV for the J/ψ meson. An initial offline selection is applied to reconstructed particles. Final-state particles are required to have $p_T > 300$ MeV, be inconsistent with originating from any PV, lie within the acceptance of the RICH detectors ($2.0 < \eta < 4.9$) and be compatible with the appropriate proton, kaon or pion mass hypotheses. Furthermore, proton candidates are required to have $10 < p < 150$ GeV, while pion and kaon candidates must have $3 < p < 150$ GeV. Candidate B^0 mesons are required to have a small χ^2_{IP} with respect to a PV, where χ^2_{IP} is defined as the change in the vertex-fit χ^2 of a given PV when reconstructed with and without including the candidate under consideration. The PV providing the smallest

χ^2_{IP} value is associated to the B^0 candidate, which is also required to be consistent with originating from this PV by applying a criterion on the angle between its momentum vector and the displacement vector from the PV to its decay vertex. To enhance the resolution of kinematic quantities, such as the diproton mass distribution $m_{p\bar{p}}$ and the two-particle mass combinations that define the DP, a kinematic fit is performed [47]. In this fit, the B^0 candidate is constrained to originate from its associated PV, and its reconstructed mass is constrained to the known B^0 mass [48].

A boosted decision tree (BDT) algorithm [49, 50] is used to suppress combinatorial background, corresponding to B^0 candidates formed by uncorrelated particles. Simulated samples of $B^0 \rightarrow p\bar{p}K^+\pi^-$ decays, generated uniformly within the available phase space of the decay, are taken as a signal proxy. The data in the mass $m_{p\bar{p}K^+\pi^-}$ region 5450–5550 MeV is used as a background proxy when training the BDT, to avoid regions containing partially reconstructed b -hadron decays. Two BDT classifiers are trained separately for Run 1 and Run 2, in order to take into account differences between the two data-taking periods.

The input variables to the BDT classifiers are: the vertex-fit χ^2 , χ^2_{IP} , a discriminating variable evaluating the pointing consistency of the reconstructed B^0 momentum to the B^0 decay vertex, the flight-distance significance of the reconstructed B^0 candidates; the maximum distance of closest approach between final-state particles, and the maximum and minimum p and p_T of the proton and antiproton. The Run 2 BDT additionally uses particle-identification variables of the final-state particles. These variables are adjusted to match the calibration data distributions and are not included in the Run 1 BDT due to the lack of suitable calibration samples [51, 52]. The selection criteria on the BDT output are chosen in order to maximise the figure of merit defined as $S/\sqrt{S+B}$, where S is the observed $B^0 \rightarrow p\bar{p}K^+\pi^-$ signal yield before any BDT selection multiplied by the efficiency of the BDT requirement evaluated using simulation, while B is the combinatorial background yield, both obtained in the $m_{p\bar{p}K^+\pi^-}$ region 5200–5360 MeV. Finally, the $\bar{D}^0 \rightarrow K^+\pi^-$, $\bar{\Lambda}_c^- \rightarrow \bar{p}K^+\pi^-$, and $\phi \rightarrow K^+K^-$ decays are vetoed by excluding the mass ranges 1835–1880 MeV, 2250–2305 MeV, and 1010–1028 MeV in the $m_{K^+\pi^-}$, $m_{\bar{p}K^+\pi^-}$, and $m_{K^+K^-}$ distributions, respectively, where the $m_{K^+K^-}$ mass has been reconstructed assigning the K^- meson mass to the π^- candidate.

3.1 Signal yield of $B^0 \rightarrow \eta_c K^+\pi^-$ decay

Prior to the DP fit, a two-dimensional extended maximum-likelihood fit to the $m_{p\bar{p}K^+\pi^-}$ and $m_{p\bar{p}}$ mass distributions is performed in order to isolate the $B^0 \rightarrow \eta_c(\rightarrow p\bar{p})K^+\pi^-$ contribution from the nonresonant (NR) component, $B^0 \rightarrow p\bar{p}K^+\pi^-$. The ranges of the fits are 5220–5340 MeV and 2908–3058 MeV for the $p\bar{p}K^+\pi^-$ and $p\bar{p}$ mass distributions, respectively.

The ROOFIT package [53] is used to perform the fit separately for the Run 1 and Run 2 data samples. The $m_{p\bar{p}K^+\pi^-}$ distributions of $B^0 \rightarrow \eta_c K^+\pi^-$ signal and $B^0 \rightarrow p\bar{p}K^+\pi^-$ NR decays are both described by a Hypatia probability density functions (PDF) [54] using the same parametrisation. The $m_{p\bar{p}}$ mass distribution of the $B^0 \rightarrow \eta_c K^+\pi^-$ signal decays is described by a relativistic Breit–Wigner (RBW) convolved with a Crystal Ball function [55], while that of the NR contribution is described by an exponential function. The $m_{p\bar{p}K^+\pi^-}$ and $m_{p\bar{p}}$ distributions of the combinatorial background are modelled using exponential functions. A possible component where η_c mesons are combined with random kaons and pions from the PV is investigated but found to be negligible. The meson peak

Table 1: Yields of the signal and background components from the two-dimensional mass fit to the $m_{p\bar{p}K^+\pi^-}$ and $m_{p\bar{p}}$ distributions for the Run 1 and Run 2 samples in the $p\bar{p}$ mass region of the η_c resonance.

Component	Yields	
	Run 1	Run 2
$B^0 \rightarrow \eta_c K^+ \pi^-$	772 ± 70	4266 ± 139
$B^0 \rightarrow p\bar{p} K^+ \pi^-$	168 ± 69	823 ± 139
Combinatorial background	361 ± 34	1665 ± 68

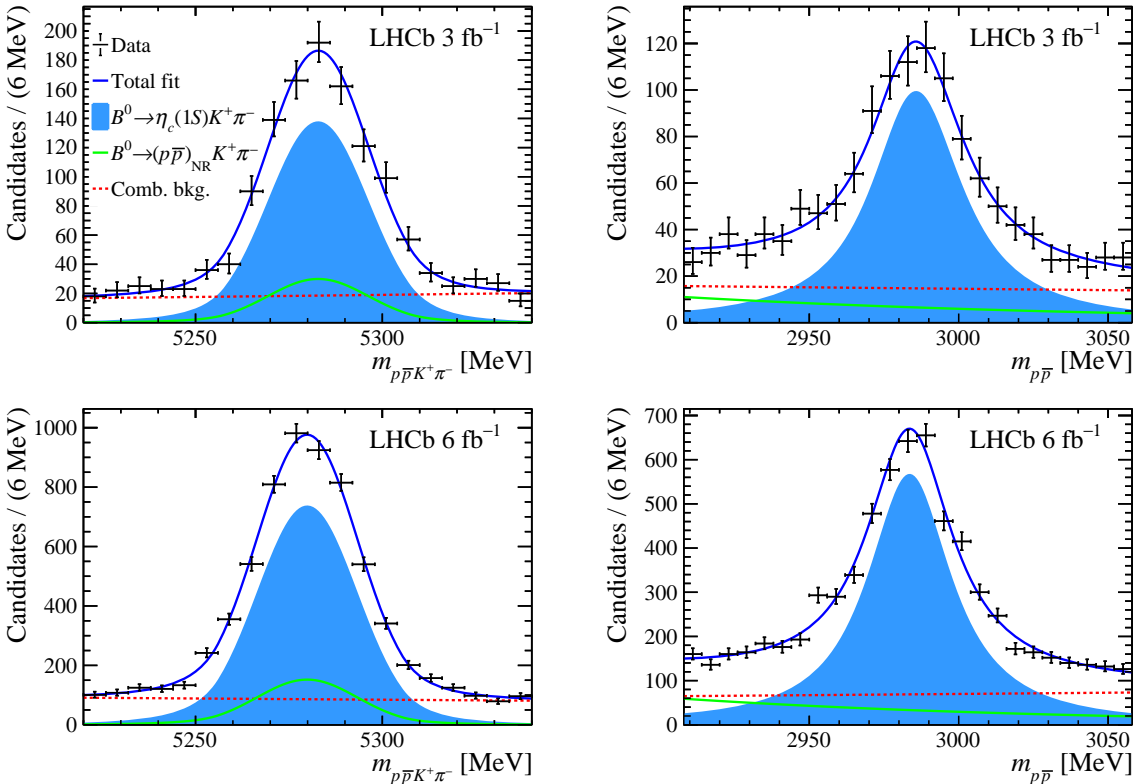


Figure 2: Results of the two-dimensional mass fit to the (left) $m_{p\bar{p}K^+\pi^-}$ and (right) $m_{p\bar{p}}$ distributions for the (top) Run 1 and (bottom) Run 2 datasets in the region of the η_c resonance.

positions, widths, slopes of the exponential functions, and yields, are free to vary in the mass fits while the shape parameters of the signal component are fixed from simulation. The yields of all fit components are reported in Table 1. Figure 2 shows the projections of the mass fits for the Run 1 and Run 2 samples.

3.2 Signal yield of the $B^0 \rightarrow J/\psi K^+ \pi^-$ decay

A similar two-dimensional fit procedure is also used to extract the yield of $B^0 \rightarrow J/\psi K^+ \pi^-$ decays. A Hypatia PDF is used to parametrise the $J/\psi \rightarrow p\bar{p}$ decay in the range 3072–3122 MeV, with the shape parameters fixed from simulation. Nonresonant contributions from $B^0 \rightarrow p\bar{p} K^+ \pi^-$ decays are not included in the fit that is used to measure $N_{J/\psi}$,

Table 2: Yields of the normalisation and background components from the two-dimensional joint mass fit to the $m_{p\bar{p}K^+\pi^-}$ and $m_{p\bar{p}}$ distributions for the Run 1 and Run 2 samples in the $p\bar{p}$ mass region of the J/ψ resonance.

Component	Yields	
	Run 1	Run 2
$B^0 \rightarrow J/\psi K^+\pi^-$	2258 ± 50	12787 ± 119
Combinatorial background	306 ± 24	1496 ± 54

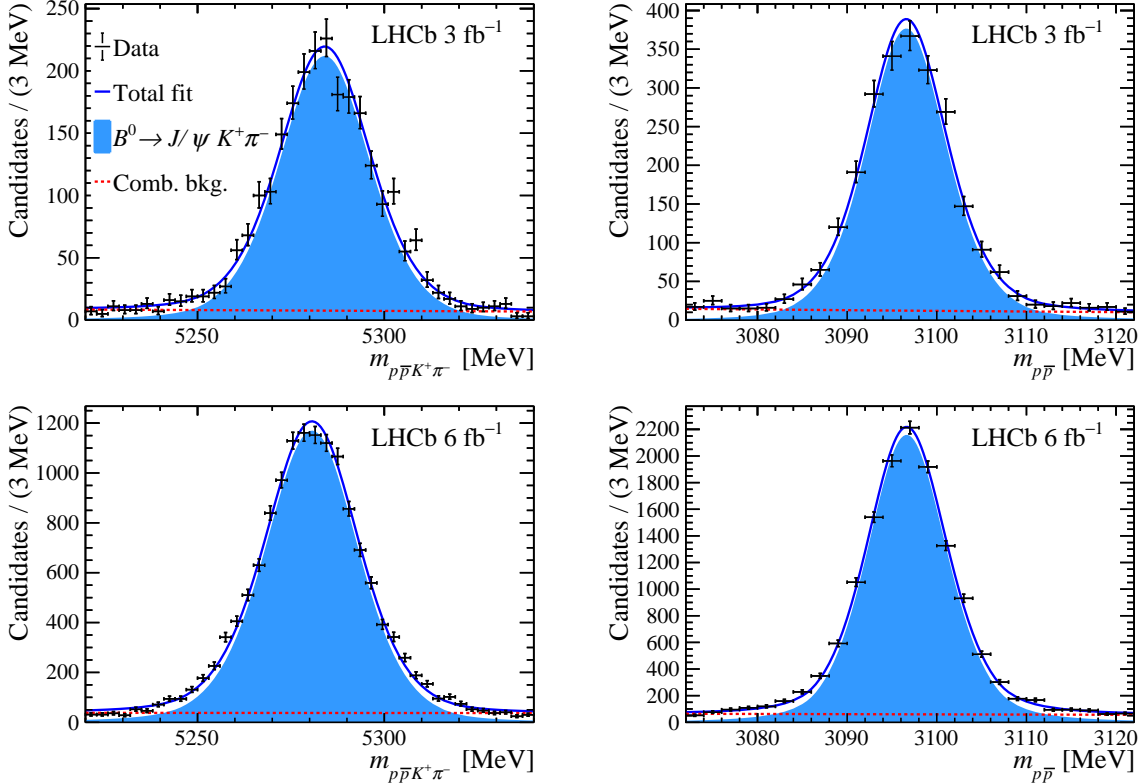


Figure 3: Results of the two-dimensional fit to the (left) $m_{p\bar{p}K^+\pi^-}$ and (right) $m_{p\bar{p}}$ distributions for the (top) Run 1 and (bottom) Run 2 datasets in the region of the J/ψ resonance.

as they are found to be insignificant. The yields of the fit components are reported in Table 2, while the results of the mass fits in the $m_{p\bar{p}}$ mass region of the J/ψ resonance is shown in Fig. 3.

4 Dalitz plot fit

Using the *sPlot* technique [56] applied to the results of the two-dimensional mass fit in the region of the η_c resonance, the background-subtracted DP is determined and shown in Fig. 4. The phase space for a three-body decay involving only pseudoscalar particles can be represented by a DP, where two of the three possible two-body mass-squared combinations, in this case $m_{K^+\pi^-}^2$ and $m_{\eta_c\pi^-}^2$, define the DP axes. Due to the sizeable

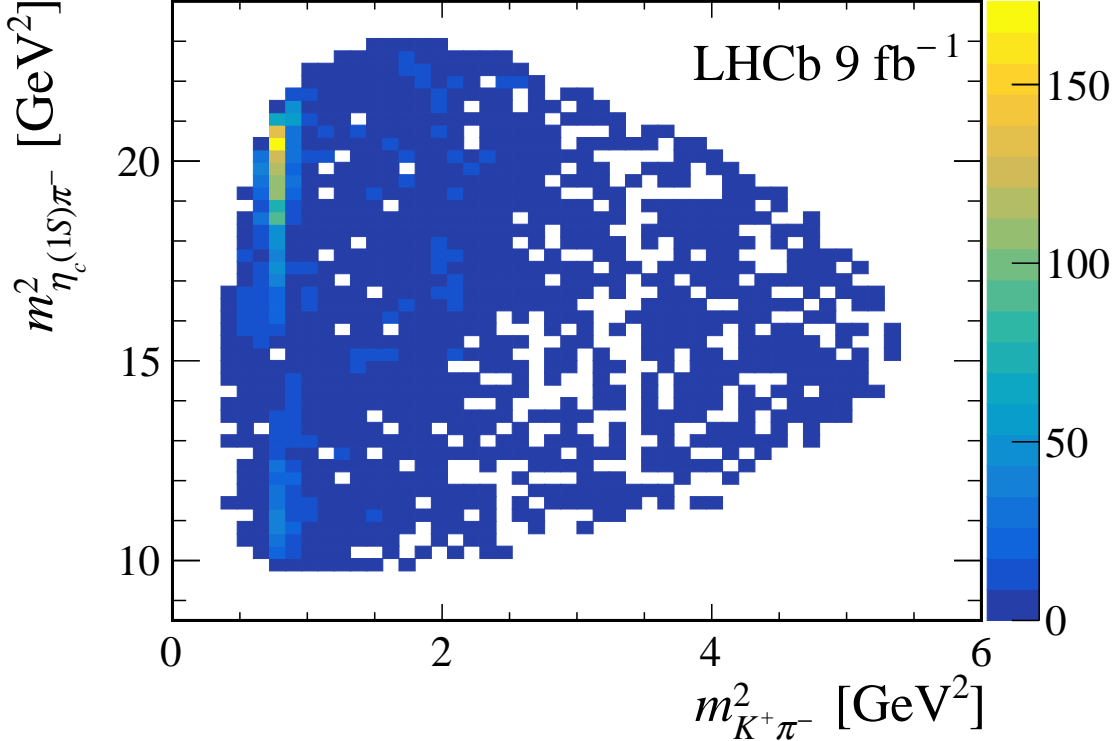


Figure 4: Background-subtracted DP distribution of the $B^0 \rightarrow \eta_c K^+ \pi^-$ decay.

natural width of the η_c meson, the p and \bar{p} momenta and energies are used instead of fixing the η_c mass to its known value [48] to compute kinematic quantities such as $m_{\eta_c K^+}^2$, $m_{\eta_c \pi^-}^2$, and the helicity angles.

The formalism used in this analysis follows the approach described in Ref. [19] where an unbinned maximum-likelihood fit on the DP is performed employing the LAURA++ package [57]. The Run 1 and Run 2 subsamples are fitted simultaneously within the JFIT framework [58], with shared free parameters in the DP fit; however, the signal and background yields, as well as the efficiency-variation maps across the phase space, are treated separately for the two datasets.

In the DP fit, the signal corresponds to $B^0 \rightarrow \eta_c K^+ \pi^-$ decays, while the background includes both combinatorial contributions and NR contributions. The likelihood function is given by

$$\mathcal{L} = e^{-\sum_k N_k} \prod_i \left[\sum_k N_k \mathcal{P}_k(m_{K^+\pi^-}^2, m_{\eta_c\pi^-}^2)_i \right], \quad (1)$$

where the index i runs over the number of candidates, while k indexes the signal and background components, with N_k representing their respective yields. The PDFs for the signal and background components are denoted by \mathcal{P}_k , for which the signal PDF is defined as the normalised squared amplitudes scaled by an efficiency model in the DP. Combinatorial and NR background shapes are extracted from the mass fits using the *sPlot* method. These histograms are also interpolated with a cubic spline before the DP fit.

To mitigate issues arising from imperfect efficiency parametrisation at the DP boundaries, a veto is applied to both the lower and upper edges of the DP, effectively excluding

regions where any of the masses, $m_{\eta_c\pi^-}$, $m_{\eta_c K^+}$, or $m_{K^+\pi^-}$, are within 70 MeV of their kinematic limits. This veto is also used in both the determination of signal and background yields and the PDF modelling the background.

The mass resolution of the $K^+\pi^-$ system is approximately 5 MeV, which is significantly smaller than the natural width of the narrowest resonance in the Dalitz plot, the $K^*(892)^0$ meson, whose width is about 50 MeV. Therefore, resolution effects are negligible and are not considered further. To ensure convergence to the global minimum, the DP fits are repeated multiple times with randomised initial parameter values.

4.1 Signal efficiency evaluation

In order to perform the DP fit of the $B^0 \rightarrow \eta_c K^+\pi^-$ decay channel, the efficiency variations across the phase space of the decay must be taken into account. Relative variations in efficiency arise from both experimental effects and selection requirements. Efficiencies are calculated on a two-dimensional map parametrised by the variables m' and θ' which are defined as

$$m' \equiv \frac{1}{\pi} \arccos \left(2 \frac{m_{K^+\pi^-} - m_{K^+\pi^-}^{\min}}{m_{K^+\pi^-}^{\max} - m_{K^+\pi^-}^{\min}} - 1 \right), \quad (2)$$

$$\theta' \equiv \frac{1}{\pi} \theta_{K^+\pi^-}, \quad (3)$$

where the helicity angle $\theta_{K^+\pi^-}$ is defined as the angle between the K^+ and the η_c particles in the $K^+\pi^-$ rest frame. This parametrisation is used to obtain a square Dalitz plot which mitigates potential issues related to the otherwise curved boundaries in the $m_{K^+\pi^-}^2$ and $m_{\eta_c\pi^-}^2$ space and the finite width of the η_c resonance. The phase-space boundaries of the $K^+\pi^-$ mass are represented by $m_{K^+\pi^-}^{\min}$ and $m_{K^+\pi^-}^{\max}$.

The efficiency distributions are computed using simulation as two-dimensional histograms in the square DP space, using the four-momenta of the final-state particles. These momenta are obtained from a fit with the selected B^0 candidates, where the B^0 mass is constrained to its known value [48] and its direction required to point towards the associated primary vertex. The efficiency distributions are calculated by applying the full event selection, where potential discrepancies arising from trigger, tracking, and B^0 -kinematic sources are found to be negligible. The effect of the vetoes in the phase space is separately accounted for by the LAURA++ package, setting the signal efficiency to zero both within the excluded regions and beyond the phase-space border restrictions. The histograms modelling the efficiency undergo a smoothing procedure through cubic-spline interpolation in order to reduce the statistical fluctuations due to the limited size of the simulated samples and are studied separately for the Run 1 and Run 2 samples.

4.2 Amplitude model with only K^{*0} resonances

The established $K^{*0} \rightarrow K^+\pi^-$ mesons, reported in Ref. [48], satisfying $m_{K^*} \lesssim m_{B^0} - m_{\eta_c}$, *i.e.* with masses within or slightly above the phase-space boundary in $B^0 \rightarrow \eta_c K^+\pi^-$ decays, serve as a guide when building the model. Only contributions that significantly improve the data description are included. This model, referred to as the baseline model, comprises the resonances shown in Table 3, with their masses and widths fixed to their known values [48], except for the $K_0^*(1430)^0$ as described later. In the DP fit, the signal

Table 3: Resonances included in the baseline model, where parameter values, uncertainties and spin-parity J^P are taken from Ref. [48]. The lineshapes used are also reported.

K^{*0} resonance	Mass [MeV]	Width [MeV]	J^P	Lineshape
$K^*(892)^0$	895.55 ± 0.20	47.3 ± 0.5	1^-	RBW
$K^*(1410)^0$	1414 ± 15	232 ± 21	1^-	RBW
$K_0^*(1430)^0$	1425 ± 50	270 ± 80	0^+	LASS
$K_2^*(1430)^0$	1432.4 ± 1.3	109 ± 5	2^+	RBW
$K^*(1680)^0$	1718 ± 18	320 ± 110	1^-	RBW
$K_0^*(1950)^0$	1957 ± 14	170 ± 50	0^+	RBW

Table 4: Parameters of the LASS function resulting from the best fit using the baseline model, where the uncertainties are statistical only.

Parameter	Value
r	$4.0 \pm 1.0 \text{ GeV}^{-1}$
a	$4.3 \pm 0.8 \text{ GeV}^{-1}$
$m_{K_0^*(1430)}$	$1434 \pm 22 \text{ MeV}$
$\Gamma_{K_0^*(1430)}$	$409 \pm 44 \text{ MeV}$

and background yields are fixed to the values obtained from the two-dimensional mass fit. The effect of the phase-space boundary cut on these yields is negligible.

The $K^*(892)^0$ resonance serves as a reference amplitude, with its magnitude fixed to unity and phase set to zero. The complex coefficients [59–61] of the remaining contributions are determined relative to those of the $K^*(892)^0$ meson. The low-mass $(K^+\pi^-)_S$ S-wave is modelled with the LASS function [62]. The scattering length (a) and the effective range (r) parametrising the slowly varying part (SVP) of the LASS function are left free to vary in the fit. The resonance mass and width are constrained with Gaussian priors centred on their known values [48]. Once the global minimum of the negative log-likelihood is reached, the four parameters reported in Table 4 are fixed to their best-fit values and then the fits are repeated. This procedure negates the recalculation of resonant lineshapes in the function minimisation loop, ensuring faster convergence. The remaining resonances in the fit are modelled using RBW lineshapes, with their Blatt–Weisskopf barrier-factor radii fixed at 4 GeV^{-1} .

A good description of the $m_{K^+\pi^-}$ and $m_{\eta_c K^+}$ mass distributions with only K^{*0} contributions is generally achieved. However, discrepancies between data and fit projections onto the $m_{\eta_c \pi^-}$ and $m_{\eta_c K^+}$ distributions are visible around $m_{\eta_c \pi^-} \sim 4.1 \text{ GeV}$ and $m_{\eta_c K^+} \sim 4.1 \text{ GeV}$, as shown in Fig. 5. The values of the magnitudes, phases and fit fractions for each contribution are reported in Table 5. A χ^2 variable is computed on the squared DP to quantitatively assess the fit quality, using an adaptive two-dimensional binning scheme that ensures at least 20 events per bin, corresponding to 324 bins. For the baseline model and binning scheme, the goodness of the fit is $\chi^2/\text{ndf} = 425/309$, where ndf is the number of degrees of freedom.

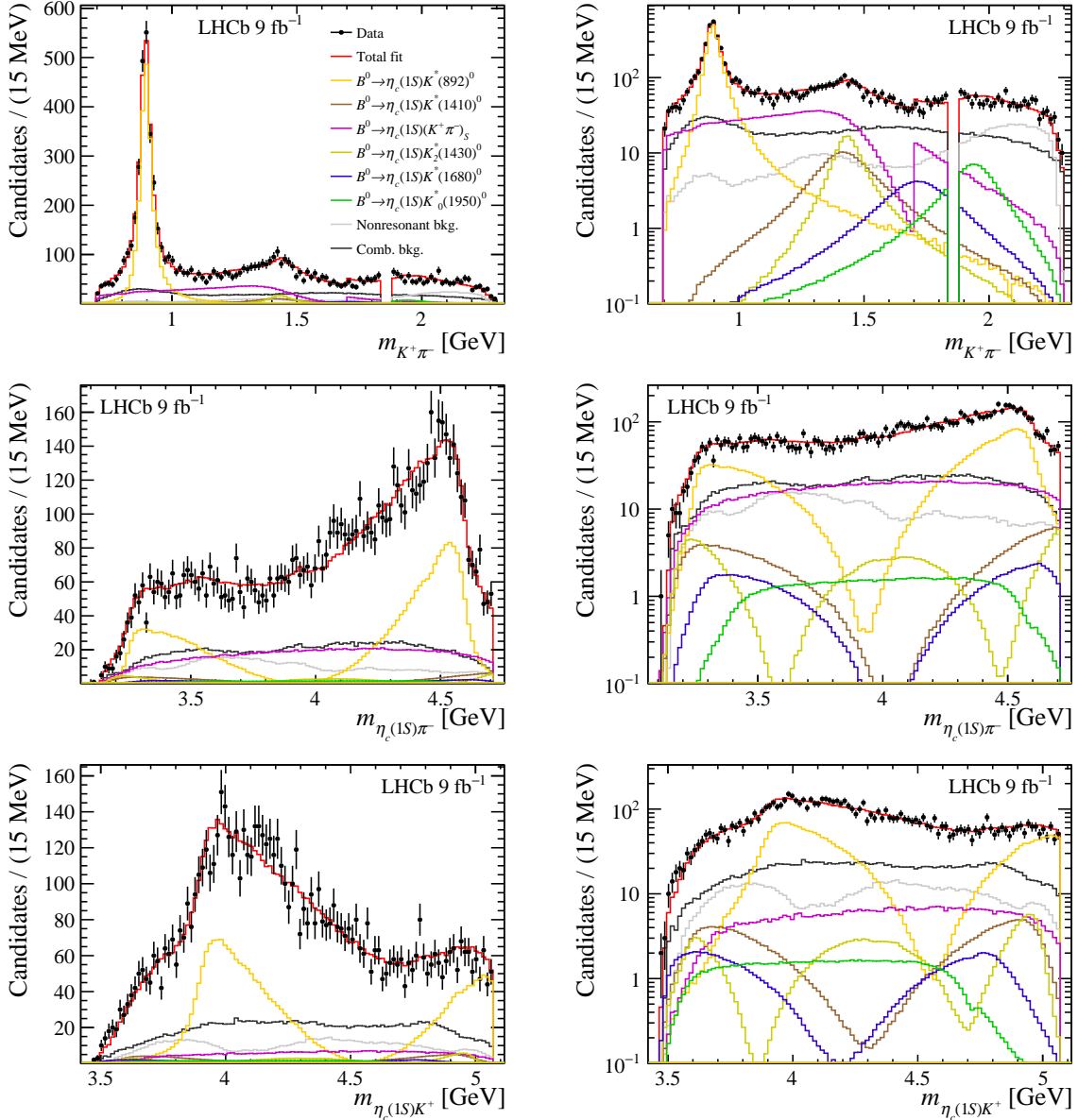


Figure 5: Projections of the $B^0 \rightarrow \eta_c K^+ \pi^-$ data and DP fit using the baseline model onto the (top) $m_{K^+ \pi^-}$, (middle) $m_{\eta_c \pi^-}$ and (bottom) $m_{\eta_c K^+}$ observables for (left) linear and (right) logarithmic vertical-axis scale. The veto of $B^0 \rightarrow p\bar{p}D^0$ decays is visible in the projections onto the $m_{K^+ \pi^-}$ observable.

4.3 Amplitude model with K^{*0} resonances and an $\eta_c \pi^-$ exotic contribution

A better description of the data, compared to the previous model, is sought by adding to the baseline model an amplitude corresponding to an exotic candidate, $T_{c\bar{c}}(4100)^- \rightarrow \eta_c \pi^-$ which is described by a RBW, in addition to the K^{*0} resonances listed in Table 3. In addition to the parameters that are free in the baseline model, the complex coefficients, and RBW mass and width of the exotic candidate are left free to vary. The strategy followed for the LASS parameters is the same as described before ensuring faster convergence times

Table 5: Magnitudes, phases and fit fractions determined from the DP fit using the baseline model, where the uncertainties are statistical only.

Amplitude	Magnitude	Phase	Fit fraction (%)
$B^0 \rightarrow \eta_c K^*(892)^0$	1 (fixed)	0 (fixed)	49.3 ± 1.2
$B^0 \rightarrow \eta_c K^*(1410)^0$	0.30 ± 0.04	-0.14 ± 0.13	4.5 ± 1.4
$B^0 \rightarrow \eta_c K_0^*(1430)^0$	0.79 ± 0.04	$+2.94 \pm 0.05$	30.8 ± 4.7
$B^0 \rightarrow \eta_c(K^+ \pi^-)_{\text{SVP}}$	0.56 ± 0.03	$+2.81 \pm 0.07$	15.4 ± 2.4
$B^0 \rightarrow \eta_c K_2^*(1430)^0$	0.28 ± 0.03	-0.73 ± 0.10	3.7 ± 0.9
$B^0 \rightarrow \eta_c K^*(1680)^0$	0.21 ± 0.05	$+0.21 \pm 0.22$	2.1 ± 0.9
$B^0 \rightarrow \eta_c K_0^*(1950)^0$	0.22 ± 0.03	$+1.53 \pm 0.29$	2.4 ± 0.5
Sum of fit fractions			108.2 ± 3.1

when an exotic contribution is included in the model. The values found from the best fit for the LASS function and the exotic candidate are reported in Table 6. A likelihood-ratio test, based on the log-likelihood difference with respect to the baseline value, $\Delta(-2 \ln \mathcal{L})$ [63], is used to compare different amplitude models. The exotic candidate is tested under two quantum-number hypotheses, repeating the DP fit for the $J^P = 0^+$ and 1^- assignments. The corresponding $\Delta(-2 \ln \mathcal{L})$ values, are 16.2 and 29.0, respectively. Thus, the model providing the best description of data, referred to as the extended fit model, is obtained with the addition of an exotic candidate with $J^P = 1^-$.

The values for the magnitude, phase and fit fraction of each contribution are reported in Table 7. Statistical uncertainties on the fit fractions are determined using large samples of pseudoexperiments generated from the fit results, thereby accounting for correlations between parameters. The mass projections of the extended model are shown in Fig. 6, for which the value of the χ^2/ndf is 401/305.

The significance of the $T_{c\bar{c}}(4100)^-$ candidate is evaluated from the value of $\Delta(-2 \ln \mathcal{L})$, assuming that this quantity follows a χ^2 distribution with degrees of freedom equal to twice the number of free parameters in its expression [64–66]. This assumption accounts for the look-elsewhere effect due to the varying mass and width of the $T_{c\bar{c}}(4100)^-$ candidate. Its validity is verified through pseudoexperiments, which test the $\Delta(-2 \ln \mathcal{L})$ distribution under the baseline hypothesis. The results confirm that this distribution is well described by a χ^2 function with 8 degrees of freedom. In the extended fit model,

Table 6: Parameters of the LASS function and the exotic $J^P = 1^-$ -candidate resulting from the best fit using the extended model.

Parameter	Value		Lineshape
r	$4.6 \pm$	1.0 GeV^{-1}	LASS
a	$4.2 \pm$	0.7 GeV^{-1}	LASS
$m_{K_0^*(1430)}$	1433 ± 19	MeV	LASS
$\Gamma_{K_0^*(1430)}$	359 ± 37	MeV	LASS
$m_{T_{c\bar{c}}(4100)^-}$	4106 ± 23	MeV	RBW
$\Gamma_{T_{c\bar{c}}(4100)^-}$	506 ± 166	MeV	RBW

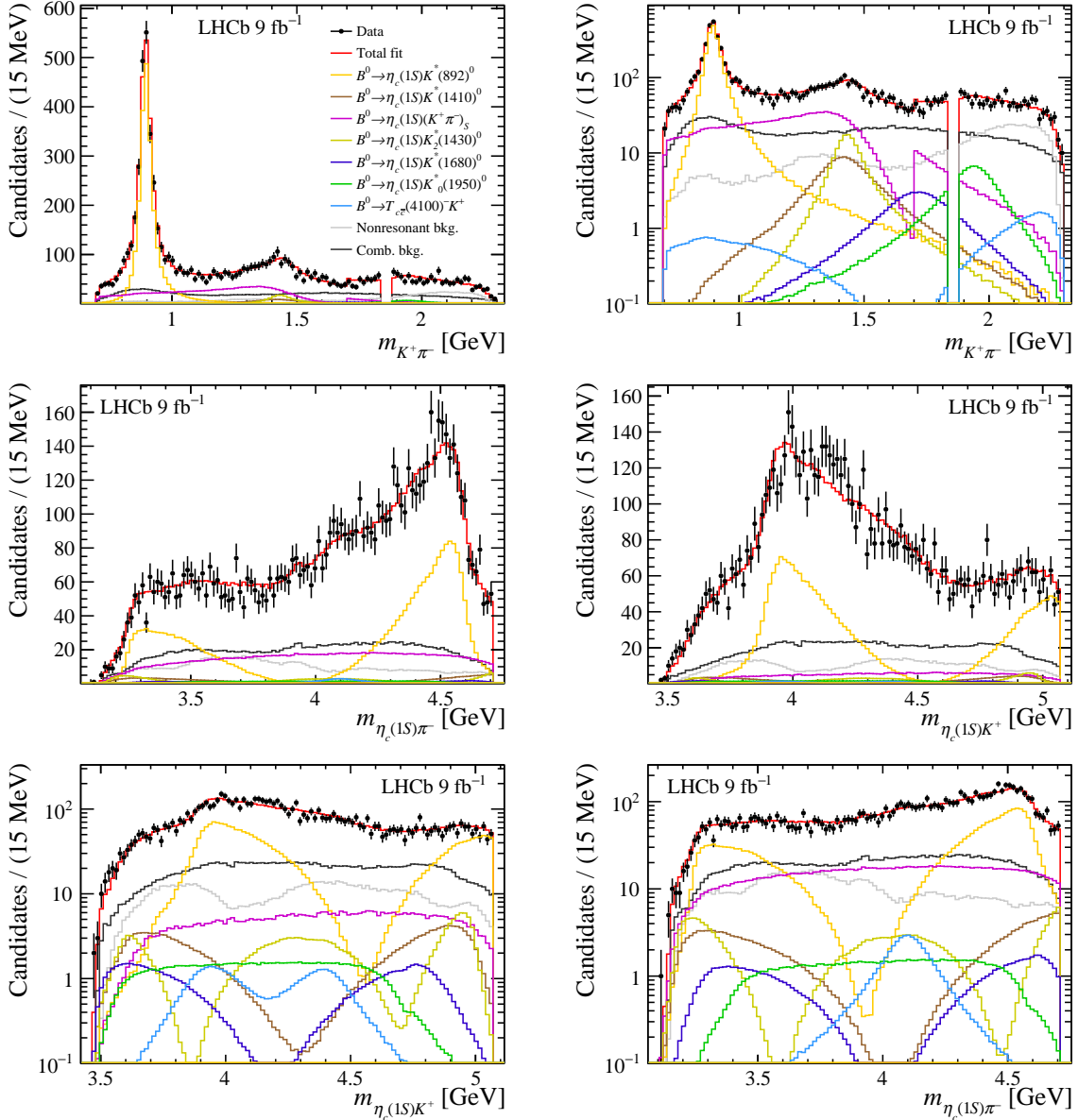


Figure 6: Projections of the $B^0 \rightarrow \eta_c K^+ \pi^-$ data and DP fit using the extended model onto the (top) $m_{K^+ \pi^-}$, (middle) $m_{\eta_c \pi^-}$ and (bottom) $m_{\eta_c K^+}$ observables for (left) linear and (right) logarithmic vertical-axis scale. The veto of $B^0 \rightarrow p\bar{p}D^0$ decays is visible in the projections onto the $m_{K^+ \pi^-}$ observable.

the statistical significance of the $T_{c\bar{c}}(4100)^-$ is found to be 3.6 standard deviations (σ), excluding systematic uncertainties. To distinguish between different J^P assignments, fits are performed under alternative J^P hypotheses. A lower limit on the significance of rejecting the $J^P = 0^+$ hypothesis is determined from the change in the log-likelihood relative to the preferred hypothesis, assuming a χ^2 distribution with one degree of freedom. This assumption is similarly validated using pseudoexperiments, which confirm that the $\Delta(-2 \ln \mathcal{L})$ distribution under the disfavoured $J^P = 0^+$ hypothesis follows the expected χ^2 behaviour. The $J^P = 0^+$ hypothesis with respect to that of $J^P = 1^-$ is statistically disfavoured at 3.2σ . However, systematic effects must be taken into account to determine

Table 7: Magnitudes, phases and fit fractions determined from the DP fit using the extended model. Uncertainties are statistical only.

Amplitude	Magnitude	Phase	Fit fraction (%)
$B^0 \rightarrow \eta_c K^*(892)^0$	1 (fixed)	0 (fixed)	49.1 ± 1.3
$B^0 \rightarrow \eta_c K^*(1410)^0$	0.28 ± 0.03	-0.04 ± 0.15	3.9 ± 0.9
$B^0 \rightarrow \eta_c K_0^*(1430)^0$	0.73 ± 0.04	-0.18 ± 0.05	26.2 ± 4.1
$B^0 \rightarrow \eta_c(K^+\pi^-)_{\text{SVP}}$	0.51 ± 0.03	$+0.31 \pm 0.07$	12.9 ± 2.0
$B^0 \rightarrow \eta_c K_2^*(1430)^0$	0.28 ± 0.03	-0.86 ± 0.11	4.0 ± 0.9
$B^0 \rightarrow \eta_c K^*(1680)^0$	0.18 ± 0.05	$+0.32 \pm 0.23$	1.5 ± 0.9
$B^0 \rightarrow \eta_c K_0^*(1950)^0$	0.21 ± 0.03	-0.92 ± 0.35	2.2 ± 0.7
$B^0 \rightarrow T_{c\bar{c}}(4100)^- K^+$	0.15 ± 0.03	-3.14 ± 0.06	1.1 ± 0.5
Sum of fit fractions			100.9 ± 3.5

the significance of the $T_{c\bar{c}}(4100)^-$ contribution and the discrimination of its quantum numbers.

4.4 Systematic uncertainties

Systematic uncertainties on the fit fractions, amplitude, and phases are evaluated by measuring the difference between the baseline value and the value obtained from different studies as detailed below.

The systematic uncertainties associated with the background model are evaluated using alternative histograms, obtained by randomly varying the bin contents within their statistical uncertainties before spline interpolation. Approximately 1000 such histograms are generated for both the combinatorial and NR background components and used to construct an equal number of pseudoexperiments, where the signal contribution is generated according to the baseline model. Each pseudoexperiment is fitted with the baseline signal model and the corresponding modified background model, and the systematic uncertainty on the fit fractions is taken as the standard deviation of the resulting distribution of best-fit values, which is well described by a Gaussian. The same pseudoexperiments are also used to estimate the significance of the $T_{c\bar{c}}(4100)^-$ state. Each is fitted twice: once with the baseline model and once with the extended model, both including the varied background maps. The resulting distribution of $\Delta(-2 \ln \mathcal{L})$ values does not follow a χ^2 distribution. A p -value is therefore determined from the fraction of fits yielding a $\Delta(-2 \ln \mathcal{L})$ greater than that observed in data, corresponding to 1.45%, or a significance of 2.5σ .

The strategy used to assess the systematic uncertainty associated to the background model is also adopted to account for the effects relating to the efficiency model. Another systematic uncertainty is associated to the veto applied to the DP borders. The DP fit is repeated removing these vetoes.

The statistical uncertainties of signal and background yields are incorporated by applying constraints with Gaussian priors and repeating the fit to account for variations within these uncertainties.

A systematic uncertainty related to the potential fit bias is determined using pseudo-experiments. Samples are generated according to the baseline fit result and fitted again.

Table 8: Significance of the extended model (with the $T_{c\bar{c}}(4100)^-$ candidate) with respect to the baseline model (without the $T_{c\bar{c}}(4100)^-$ candidate) for the main sources of systematic uncertainty.

Source	Significance
Background parametrisation	2.5σ
Efficiency parametrisation	4.1σ
DP-border veto	3.2σ
Fixed yields	3.2σ
η_c natural width	3.0σ
Fixed K^{*0} lineshape parameters	3.2σ
$K^+\pi^-$ S-wave	4.5σ

The associated error is calculated as the squared sum of the residuals and the standard deviation.

The kinematic variables used in the DP fit are computed from the B^0 -meson and final-state-particle four-momenta. In order to associate a systematic uncertainty to the η_c natural width, the DP fits are repeated with kinematic variables that are recomputed assigning to the η_c mass the values $m_{\eta_c} \pm \Gamma_{\eta_c}/2$, where m_{η_c} and Γ_{η_c} are the mass and natural width of the η_c meson, respectively, obtained from the mass fits reported in Sec. 3.1.

In the baseline model the K^{*0} resonances are modelled by RBW functions with their mass and width parameters fixed to known values [48], and with fixed Blatt–Weisskopf barrier factor radii. The uncertainties related to this choice are determined by varying simultaneously and randomly the masses and widths within their uncertainties and, separately, by changing the radii between 3 and 5 GeV^{-1} .

The LASS model used to parametrise the low-mass $K^+\pi^-$ S-wave in the baseline fit is replaced with $K_0^*(1430)^0$ and $K_0^*(700)^0$ resonances parametrised by RBW functions, and a NR S-wave $K^+\pi^-$ component parametrised with a uniform amplitude.

When including these sources of systematic uncertainties, summarised in Table 8, the $T_{c\bar{c}}(4100)^-$ contribution is not found to be significant. Only the significances that deviate most from the nominal value are shown and the background parametrisation is found to be dominant. For this reason, systematic uncertainties associated to the mass and width of the $T_{c\bar{c}}(4100)^-$ candidate, and on the discrimination between quantum-number hypotheses, are not assigned.

The baseline model is therefore used to compute the branching fractions of the K^{*0} contributions in order to characterise the $B^0 \rightarrow \eta_c K^+\pi^-$ decay channel. To this end, the extended model is also considered as an alternative to the baseline model, with associated systematic uncertainties. The addition of a resonance decaying to $\eta_c K^+$ was initially considered, but it was consistently found to be less significant than the one decaying to $\eta_c \pi^-$. Therefore, it was not pursued further. The values for the fit fractions of the K^{*0} components and their interference fit fractions, together with their associated systematic uncertainties, are reported in Table 9, while the magnitudes and phases are given in Table 10.

Table 9: Symmetric matrix of the fit fractions and interference fit fractions (%) resulting from the fit using the baseline model, where the quoted uncertainties are statistical and systematic, respectively. Entries marked with a dash correspond to instances where the modulus of the interference fit fraction is found to be less than $10^{-4}\%$.

	$\eta_c K^*(892)^0$	$\eta_c K^*(1410)^0$	$\eta_c K_0^*(1430)^0$	$\eta_c(K^+ \pi^-)_{\text{SVP}}$	$\eta_c K_2^*(1430)^0$	$\eta_c K^*(1680)^0$	$\eta_c K_0^*(1950)^0$
$\eta_c K^*(892)^0$	$49.3 \pm 1.2^{+3.8}_{-3.4}$	$-2.1 \pm 1.8^{+3.1}_{-3.3}$	—	—	—	$0.8 \pm 1.2^{+3.7}_{-4.5}$	—
$\eta_c K^*(1410)^0$	—	$4.5 \pm 1.4^{+3.2}_{-3.1}$	—	—	—	$-3.2 \pm 1.5^{+6.5}_{-2.3}$	—
$\eta_c K_0^*(1430)^0$	—	$30.8 \pm 4.7^{+5.5}_{-4.3}$	$-10.8 \pm 1.3^{+1.9}_{-1.5}$	—	—	—	$7.0 \pm 10.3^{+7.9}_{-8.6}$
$\eta_c(K^+ \pi^-)_{\text{SVP}}$	—	—	$15.4 \pm 2.4^{+2.7}_{-2.2}$	—	—	—	—
$\eta_c K_2^*(1430)^0$	—	—	—	$3.7 \pm 0.9^{+1.3}_{-2.0}$	—	—	—
$\eta_c K^*(1680)^0$	—	—	—	—	$2.1 \pm 0.9^{+1.3}_{-1.7}$	—	—
$\eta_c K_0^*(1950)^0$	—	—	—	—	$2.4 \pm 0.5^{+2.7}_{-2.4}$	—	—

Table 10: Magnitudes and phases determined from the DP fit using the baseline model, where the uncertainties are statistical and systematic, respectively.

Amplitude	Magnitude	Phase
$B^0 \rightarrow \eta_c K^*(892)^0$	1 (fixed)	0 (fixed)
$B^0 \rightarrow \eta_c K^*(1410)^0$	$0.30 \pm 0.04^{+0.06}_{-0.14}$	$-0.14 \pm 0.13^{+0.57}_{-0.53}$
$B^0 \rightarrow \eta_c K_0^*(1430)^0$	$0.79 \pm 0.04^{+0.17}_{-0.06}$	$+2.94 \pm 0.05^{+0.09}_{-0.10}$
$B^0 \rightarrow \eta_c (K^+ \pi^-)_{\text{SVP}}$	$0.56 \pm 0.03^{+0.15}_{-0.07}$	$+2.81 \pm 0.07^{+0.07}_{-0.09}$
$B^0 \rightarrow \eta_c K_2^*(1430)^0$	$0.28 \pm 0.03^{+0.03}_{-0.07}$	$-0.73 \pm 0.10^{+0.19}_{-0.23}$
$B^0 \rightarrow \eta_c K^*(1680)^0$	$0.21 \pm 0.05^{+0.05}_{-0.09}$	$+0.21 \pm 0.22^{+0.59}_{-0.31}$
$B^0 \rightarrow \eta_c K_0^*(1950)^0$	$0.22 \pm 0.03^{+0.09}_{-0.08}$	$+1.53 \pm 0.29^{+0.73}_{-0.55}$

5 Branching fraction measurement

The measurement of the inclusive $B^0 \rightarrow \eta_c K^+ \pi^-$ branching fraction is performed relative to the normalisation channel $B^0 \rightarrow J/\psi K^+ \pi^-$. The absolute branching fraction of the $B^0 \rightarrow \eta_c K^+ \pi^-$ decay can then be calculated using the relation

$$\mathcal{B}(B^0 \rightarrow \eta_c K^+ \pi^-) = \mathcal{B}(B^0 \rightarrow J/\psi K^+ \pi^-) \frac{\mathcal{B}(J/\psi \rightarrow p\bar{p})}{\mathcal{B}(\eta_c \rightarrow p\bar{p})} \frac{N_{\eta_c}}{N_{J/\psi}} \frac{\epsilon_{J/\psi}}{\epsilon_{\eta_c}}, \quad (4)$$

where $\mathcal{B}(B^0 \rightarrow J/\psi K^+ \pi^-) = (1.15 \pm 0.05) \times 10^{-3}$, $\mathcal{B}(J/\psi \rightarrow p\bar{p}) = (2.120 \pm 0.029) \times 10^{-3}$ and $\mathcal{B}(\eta_c \rightarrow p\bar{p}) = (1.33 \pm 0.11) \times 10^{-3}$ are taken as external inputs [48]. The values N_{η_c} and $N_{J/\psi}$ are the respective yields of the $B^0 \rightarrow \eta_c K^+ \pi^-$ and $B^0 \rightarrow J/\psi K^+ \pi^-$ contributions, as reported in Tables 1 and 2, while $\epsilon_{J/\psi}$ and ϵ_{η_c} are the selection efficiencies of the signal and normalisation channel calculated from simulation.

Selection efficiencies are determined from the $B^0 \rightarrow \eta_c K^+ \pi^-$ and $B^0 \rightarrow J/\psi K^+ \pi^-$ simulated samples, both selected using the same criteria as applied to data. Weights are applied to the simulated candidates to correct for minor discrepancies with respect to data, based on track multiplicity, B^0 kinematic distributions, and the respective DP distributions. Discrepancies due to the trigger responses are investigated and found to be negligible. The ratio of efficiencies is given by $\epsilon_{J/\psi}/\epsilon_{\eta_c} = 0.945 \pm 0.004$ for Run 1 and $\epsilon_{J/\psi}/\epsilon_{\eta_c} = 0.948 \pm 0.003$ for Run 2, where the uncertainties are statistical.

Systematic uncertainties on the branching fraction measurement are evaluated by recomputing the signal and normalisation yields, along with their efficiency ratios, for each source of uncertainty. The difference of the resulting branching fraction from the baseline value is taken as the associated systematic uncertainty. The overall systematic uncertainty is calculated by combining all contributions in quadrature. The contribution arising from fixing the parameters of the Hypatia PDFs used to parametrise the B^0 and J/ψ components, as well as the Crystal Ball PDF for the η_c , is evaluated by repeating the fit with parameter values varied according to a multivariate normal distribution. To assess a systematic uncertainty for the model used to describe the mass resolution, the fits are repeated by replacing the Hypatia PDFs with Crystal Ball PDFs. The convolution of the RBW with a Crystal Ball PDF is replaced by a Voigtian PDF, where the parameters are fixed based on simulation. The $m_{p\bar{p}}$ distribution of the NR component, originally parametrised with an exponential function, is instead modelled with a linear function. The systematic uncertainty related to the choice of the mass ranges in the two-dimensional fit is

Table 11: Systematic uncertainties on the $B^0 \rightarrow \eta_c K^+ \pi^-$ branching fraction. Statistical uncertainties are also reported for comparison.

Source	$\sigma_{\mathcal{B}(B^0 \rightarrow \eta_c K^+ \pi^-)} [10^{-4}]$	
	Run 1	Run 2
Shape parameters	0.05	0.05
Resolution and NR $p\bar{p}$ model	0.18	0.22
Mass windows	0.41	0.15
Total systematic uncertainty	0.45	0.27
Statistical uncertainty	0.53	0.22

Table 12: Product branching fractions for intermediate K^{*0} resonances decaying to $K^+ \pi^-$ contributing to the $B^0 \rightarrow \eta_c K^{*0} (\rightarrow K^+ \pi^-)$ decay, $\mathcal{B}(B^0 \rightarrow \eta_c K^{*0}) \times \mathcal{B}(K^{*0} \rightarrow K^+ \pi^-)$. The quoted uncertainties are statistical, from the inclusive branching fraction of $B^0 \rightarrow \eta_c K^+ \pi^-$, from the intermediate fit fraction and from the charmonium branching fractions of $\eta_c \rightarrow p\bar{p}$ and $J/\psi \rightarrow p\bar{p}$, respectively.

Decay	Branching fraction [10^{-5}]
$B^0 \rightarrow \eta_c K^*(892)^0 (\rightarrow K^+ \pi^-)$	$28.69 \pm 1.21 \pm 1.13^{+2.21}_{-1.98} \pm 2.71$
$B^0 \rightarrow \eta_c K^*(1410)^0 (\rightarrow K^+ \pi^-)$	$2.62 \pm 0.82 \pm 0.10^{+1.86}_{-1.80} \pm 0.25$
$B^0 \rightarrow \eta_c K_0^*(1430)^0 (\rightarrow K^+ \pi^-)$	$17.92 \pm 2.80 \pm 0.71^{+3.26}_{-2.56} \pm 1.69$
$B^0 \rightarrow \eta_c (K^+ \pi^-)_{\text{SVP}}$	$8.96 \pm 1.42 \pm 0.35^{+1.63}_{-1.28} \pm 0.84$
$B^0 \rightarrow \eta_c K_2^*(1430)^0 (\rightarrow K^+ \pi^-)$	$2.15 \pm 0.53 \pm 0.08^{+0.76}_{-1.16} \pm 0.20$
$B^0 \rightarrow \eta_c K^*(1680)^0 (\rightarrow K^+ \pi^-)$	$1.22 \pm 0.52 \pm 0.05^{+0.76}_{-0.99} \pm 0.12$
$B^0 \rightarrow \eta_c K_0^*(1950)^0 (\rightarrow K^+ \pi^-)$	$1.40 \pm 0.29 \pm 0.06^{+1.57}_{-1.40} \pm 0.13$

evaluated by performing fits with alternative ranges. Table 11 summarises the systematic uncertainties.

The measured values of the branching fraction $\mathcal{B}(B^0 \rightarrow \eta_c K^+ \pi^-)$ are $(6.10 \pm 0.53 \pm 0.45 \pm 0.58) \times 10^{-4}$ for Run 1 and $(5.77 \pm 0.22 \pm 0.27 \pm 0.55) \times 10^{-4}$ for Run 2. This leads to the combined value

$$\mathcal{B}(B^0 \rightarrow \eta_c K^+ \pi^-) = (5.82 \pm 0.20 \pm 0.23 \pm 0.55) \times 10^{-4},$$

where the first uncertainty is statistical, the second systematic, and the third is due to the limited knowledge of the external branching fractions. The combined value is obtained as the weighted average of the Run 1 and Run 2 results. This result is in agreement with the world average [48] and with the previous LHCb result [19]. The product branching fractions for the intermediate states contributing to the $B^0 \rightarrow \eta_c K^{*0} (\rightarrow K^+ \pi^-)$ decays listed in Table 12, are determined by scaling the inclusive branching fraction $\mathcal{B}(B^0 \rightarrow \eta_c K^+ \pi^-)$ by the fit fractions of each intermediate state with the baseline model reported in Table 9.

6 Conclusion

An amplitude analysis of the $B^0 \rightarrow \eta_c(1S)K^+\pi^-$ decay channel is performed using the dataset collected by LHCb in Run 1 and 2, corresponding to an integrated luminosity of 9 fb^{-1} . While a better description of the data is achieved when including a charged exotic charmonium-like $T_{c\bar{c}}(4100)^-$ candidate decaying to $\eta_c(1S)\pi^-$, the contribution is not significant when systematic uncertainties are taken into account.

A measurement of the inclusive $B^0 \rightarrow \eta_c(1S)K^+\pi^-$ branching fraction is also performed, as well as the branching fraction measurements of the intermediate K^{*0} resonances contributing to the decay. The results of this analysis, using a data sample size that is approximately doubled with respect to the previous study, supersede those obtained in Ref. [19].

Acknowledgements

We express our gratitude to our colleagues in the CERN accelerator departments for the excellent performance of the LHC. We thank the technical and administrative staff at the LHCb institutes. We acknowledge support from CERN and from the national agencies: ARC (Australia); CAPES, CNPq, FAPERJ and FINEP (Brazil); MOST and NSFC (China); CNRS/IN2P3 (France); BMBF, DFG and MPG (Germany); INFN (Italy); NWO (Netherlands); MNiSW and NCN (Poland); MCID/IFA (Romania); MICIU and AEI (Spain); SNSF and SER (Switzerland); NASU (Ukraine); STFC (United Kingdom); DOE NP and NSF (USA). We acknowledge the computing resources that are provided by ARDC (Australia), CBPF (Brazil), CERN, IHEP and LZU (China), IN2P3 (France), KIT and DESY (Germany), INFN (Italy), SURF (Netherlands), Polish WLCG (Poland), IFIN-HH (Romania), PIC (Spain), CSCS (Switzerland), and GridPP (United Kingdom). We are indebted to the communities behind the multiple open-source software packages on which we depend. Individual groups or members have received support from Key Research Program of Frontier Sciences of CAS, CAS PIFI, CAS CCEPP, Fundamental Research Funds for the Central Universities, and Sci. & Tech. Program of Guangzhou (China); Minciencias (Colombia); EPLANET, Marie Skłodowska-Curie Actions, ERC and NextGenerationEU (European Union); A*MIDEX, ANR, IPhU and Labex P2IO, and Région Auvergne-Rhône-Alpes (France); Alexander-von-Humboldt Foundation (Germany); ICSC (Italy); Severo Ochoa and María de Maeztu Units of Excellence, GVA, XuntaGal, GENCAT, InTalent-Inditex and Prog. Atracción Talento CM (Spain); SRC (Sweden); the Leverhulme Trust, the Royal Society and UKRI (United Kingdom).

References

- [1] M. Gell-Mann, *A schematic model of baryons and mesons*, *Phys. Lett.* **8** (1964) 214.
- [2] G. Zweig, *An SU_3 model for strong interaction symmetry and its breaking; Version 1* **CERN-TH-401**, CERN, Geneva, 1964.
- [3] Belle collaboration, S.-K. Choi *et al.*, *Observation of a narrow charmonium-like state in exclusive $B^\pm \rightarrow K^\pm\pi^+\pi^-J/\psi$ decays*, *Phys. Rev. Lett.* **91** (2003) 262001, [arXiv:hep-ex/0309032](https://arxiv.org/abs/hep-ex/0309032).

- [4] Belle collaboration, A. Bondar *et al.*, *Observation of two charged bottomonium-like resonances in $Y(5S)$ decays*, Phys. Rev. Lett. **108** (2012) 122001, [arXiv:1110.2251](#).
- [5] Belle collaboration, K. Abe *et al.*, *Observation of a near-threshold $\omega J/\psi$ mass enhancement in exclusive $B \rightarrow K\omega J/\psi$ decays*, Phys. Rev. Lett. **94** (2005) 182002, [arXiv:hep-ex/0408126](#).
- [6] CLEO collaboration, T. E. Coan *et al.*, *Charmonium decays of $Y(4260)$, $\psi(4160)$ and $\psi(4040)$* , Phys. Rev. Lett. **96** (2006) 162003, [arXiv:hep-ex/0602034](#).
- [7] CDF collaboration, T. Aaltonen *et al.*, *Observation of the $Y(4140)$ Structure in the $J/\psi\phi$ Mass Spectrum in $B^\pm \rightarrow J/\psi\phi K^\pm$ Decays*, Mod. Phys. Lett. **A32** (2017) 1750139, [arXiv:1101.6058](#).
- [8] M. Karliner and J. L. Rosner, *New exotic meson and baryon resonances from doubly heavy hadronic molecules*, Phys. Rev. Lett. **115** (2015) 122001, [arXiv:1506.06386](#).
- [9] L. Maiani, F. Piccinini, A. D. Polosa, and V. Riquer, *Diquark-antidiquarks with hidden or open charm and the nature of $X(3872)$* , Phys. Rev. **D71** (2005) 014028, [arXiv:hep-ph/0412098](#).
- [10] L. Maiani, A. D. Polosa, and V. Riquer, *The new pentaquarks in the diquark model*, Phys. Lett. **B749** (2015) 289, [arXiv:1507.04980](#).
- [11] S. Dubynskiy and M. B. Voloshin, *Hadro-charmonium*, Phys. Lett. **B666** (2008) 344, [arXiv:0803.2224](#).
- [12] D. V. Bugg, *An explanation of Belle states $Z_b(10610)$ and $Z_b(10650)$* , EPL **96** (2011) 11002, [arXiv:1105.5492](#).
- [13] P. Pakhlov and T. Uglow, *Charged charmonium-like $Z^+(4430)$ from rescattering in conventional B decays*, Phys. Lett. **B748** (2015) 183, [arXiv:1408.5295](#).
- [14] BESIII collaboration, M. Ablikim *et al.*, *Observation of a charged charmoniumlike structure in $e^+e^- \rightarrow \pi^+\pi^- J/\psi$ at $\sqrt{s} = 4.26$ GeV*, Phys. Rev. Lett. **110** (2013) 252001, [arXiv:1303.5949](#).
- [15] Belle collaboration, Z. Q. Liu *et al.*, *Study of $e^+e^- \rightarrow \pi^+\pi^- J/\psi$ and observation of a charged charmoniumlike state at Belle*, Phys. Rev. Lett. **110** (2013) 252002, Erratum **111** (2013) 019901, [arXiv:1304.0121](#).
- [16] T. Xiao, S. Dobbs, A. Tomaradze, and K. K. Seth, *Observation of the charged hadron $Z_c^\pm(3900)$ and evidence for the neutral $Z_c^0(3900)$ in $e^+e^- \rightarrow \pi\pi J/\psi$ at $\sqrt{s} = 4170$ MeV*, Phys. Lett. **B727** (2013) 366, [arXiv:1304.3036](#).
- [17] M. B. Voloshin, *$Z_c(3900)$ —what is inside?*, Phys. Rev. **D87** (2013) 091501, [arXiv:1304.0380](#).
- [18] E. Braaten, *How the $Z_c(3900)$ reveals the spectra of charmonium hybrids and tetraquarks*, Phys. Rev. Lett. **111** (2013) 162003, [arXiv:1305.6905](#).

- [19] LHCb collaboration, R. Aaij *et al.*, *Evidence for an $\eta_c(1S)\pi^-$ resonance in $B^0 \rightarrow \eta_c(1S)K^+\pi^-$ decays*, *Eur. Phys. J. C* **78** (2018) 1019, [arXiv:1809.07416](#).
- [20] H. Sundu, S. S. Agaev, and K. Azizi, *New charged resonance $Z_c^-(4100)$: the spectroscopic parameters and width*, *Eur. Phys. J. C* **79** (2019) 215, [arXiv:1812.10094](#).
- [21] J. Wu, X. Liu, Y.-R. Liu, and S.-L. Zhu, *Systematic studies of charmonium-, bottomonium-, and B_c -like tetraquark states*, *Phys. Rev. D* **99** (2019) 014037, [arXiv:1810.06886](#).
- [22] M. B. Voloshin, *$Z_c(4100)$ and $Z_c(4200)$ as hadrocharmonium*, *Phys. Rev. D* **98** (2018) 094028, [arXiv:1810.08146](#).
- [23] Belle collaboration, K. Chilikin *et al.*, *Observation of a new charged charmoniumlike state in $\bar{B}^0 \rightarrow J/\psi K^-\pi^+$ decays*, *Phys. Rev. D* **90** (2014) 112009, [arXiv:1408.6457](#).
- [24] LHCb collaboration, R. Aaij *et al.*, *Model-independent observation of exotic contributions to $B^0 \rightarrow J/\psi K^+\pi^-$ decays*, *Phys. Rev. Lett.* **122** (2019) 152002, [arXiv:1901.05745](#).
- [25] X. Cao and J.-P. Dai, *Spin parity of $Z_c^-(4100)$, $Z_1^+(4050)$, and $Z_2^+(4250)$* , *Phys. Rev. D* **100** (2019) 054004, [arXiv:1811.06434](#).
- [26] Belle collaboration, R. Mizuk *et al.*, *Observation of two resonancelike structures in the $\pi^+\chi_{c1}$ mass distribution in exclusive $\bar{B}^0 \rightarrow K^-\pi^+\chi_{c1}$ decays*, *Phys. Rev. D* **78** (2008) 072004, [arXiv:0806.4098](#).
- [27] Q. Zhao, *Some insights into the newly observed $Z_c(4100)$ in $B^0 \rightarrow \eta_c K^+\pi^-$ by LHCb*, [arXiv:1811.05357](#).
- [28] Belle collaboration, K. Chilikin *et al.*, *Evidence for $B^+ \rightarrow h_c K^+$ and observation of $\eta_c(2S) \rightarrow p\bar{p}\pi^+\pi^-$* , *Phys. Rev. D* **100** (2019) 012001, [arXiv:1903.06414](#).
- [29] R. H. Dalitz, *On the analysis of τ -meson data and the nature of the τ -meson*, *Phil. Mag. Ser. 7* **44** (1953) 1068.
- [30] LHCb collaboration, A. A. Alves Jr. *et al.*, *The LHCb detector at the LHC*, *JINST* **3** (2008) S08005.
- [31] LHCb collaboration, R. Aaij *et al.*, *LHCb detector performance*, *Int. J. Mod. Phys. A* **30** (2015) 1530022, [arXiv:1412.6352](#).
- [32] R. Aaij *et al.*, *Performance of the LHCb Vertex Locator*, *JINST* **9** (2014) P09007, [arXiv:1405.7808](#).
- [33] R. Arink *et al.*, *Performance of the LHCb Outer Tracker*, *JINST* **9** (2014) P01002, [arXiv:1311.3893](#).
- [34] P. d'Argent *et al.*, *Improved performance of the LHCb Outer Tracker in LHC Run 2*, *JINST* **12** (2017) P11016, [arXiv:1708.00819](#).
- [35] M. Adinolfi *et al.*, *Performance of the LHCb RICH detector at the LHC*, *Eur. Phys. J.* **C73** (2013) 2431, [arXiv:1211.6759](#).

- [36] A. A. Alves Jr. *et al.*, *Performance of the LHCb muon system*, *JINST* **8** (2013) P02022, [arXiv:1211.1346](https://arxiv.org/abs/1211.1346).
- [37] R. Aaij *et al.*, *The LHCb trigger and its performance in 2011*, *JINST* **8** (2013) P04022, [arXiv:1211.3055](https://arxiv.org/abs/1211.3055).
- [38] V. V. Gligorov and M. Williams, *Efficient, reliable and fast high-level triggering using a bonsai boosted decision tree*, *JINST* **8** (2013) P02013, [arXiv:1210.6861](https://arxiv.org/abs/1210.6861).
- [39] T. Likhomanenko *et al.*, *LHCb topological trigger reoptimization*, *J. Phys. Conf. Ser.* **664** (2015) 082025, [arXiv:1510.00572](https://arxiv.org/abs/1510.00572).
- [40] T. Sjöstrand, S. Mrenna, and P. Skands, *A brief introduction to PYTHIA 8.1*, *Comput. Phys. Commun.* **178** (2008) 852, [arXiv:0710.3820](https://arxiv.org/abs/0710.3820).
- [41] I. Belyaev *et al.*, *Handling of the generation of primary events in Gauss, the LHCb simulation framework*, *J. Phys. Conf. Ser.* **331** (2011) 032047.
- [42] D. J. Lange, *The EvtGen particle decay simulation package*, *Nucl. Instrum. Meth. A* **462** (2001) 152.
- [43] N. Davidson, T. Przedzinski, and Z. Was, *PHOTOS interface in C++: Technical and physics documentation*, *Comput. Phys. Commun.* **199** (2016) 86, [arXiv:1011.0937](https://arxiv.org/abs/1011.0937).
- [44] Geant4 collaboration, J. Allison *et al.*, *Geant4 developments and applications*, *IEEE Trans. Nucl. Sci.* **53** (2006) 270; Geant4 collaboration, S. Agostinelli *et al.*, *Geant4: A simulation toolkit*, *Nucl. Instrum. Meth. A* **506** (2003) 250.
- [45] M. Clemencic *et al.*, *The LHCb simulation application, Gauss: Design, evolution and experience*, *J. Phys. Conf. Ser.* **331** (2011) 032023.
- [46] D. Müller, M. Clemencic, G. Corti, and M. Gersabeck, *ReDecay: A novel approach to speed up the simulation at LHCb*, *Eur. Phys. J. C* **78** (2018) 1009, [arXiv:1810.10362](https://arxiv.org/abs/1810.10362).
- [47] W. D. Hulsbergen, *Decay chain fitting with a Kalman filter*, *Nucl. Instrum. Meth. A* **552** (2005) 566, [arXiv:physics/0503191](https://arxiv.org/abs/physics/0503191).
- [48] Particle Data Group, S. Navas *et al.*, *Review of particle physics*, *Phys. Rev. D* **110** (2024) 030001.
- [49] Y. Freund and R. E. Schapire, *A decision-theoretic generalization of on-line learning and an application to boosting*, *J. Comput. Syst. Sci.* **55** (1997) 119.
- [50] L. Breiman, J. H. Friedman, R. A. Olshen, and C. J. Stone, *Classification and regression trees*, Wadsworth international group, Belmont, California, USA, 1984.
- [51] R. Aaij *et al.*, *Selection and processing of calibration samples to measure the particle identification performance of the LHCb experiment in Run 2*, *Eur. Phys. J. Tech. Instr.* **6** (2019) 1, [arXiv:1803.00824](https://arxiv.org/abs/1803.00824).
- [52] L. Anderlini *et al.*, *The PIDCalib package*, [LHCb-PUB-2016-021](https://lhcb-pub-2016-021.lhcb.cern.ch/), 2016.

- [53] W. Verkerke and D. P. Kirkby, *The RooFit toolkit for data modeling*, eConf **C0303241** (2003) MOLT007, [arXiv:physics/0306116](https://arxiv.org/abs/physics/0306116).
- [54] D. Martínez Santos and F. Dupertuis, *Mass distributions marginalized over per-event errors*, Nucl. Instrum. Meth. **A764** (2014) 150, [arXiv:1312.5000](https://arxiv.org/abs/1312.5000).
- [55] T. Skwarnicki, *A study of the radiative cascade transitions between the Upsilon-prime and Upsilon resonances*, PhD thesis, Institute of Nuclear Physics, Krakow, 1986, DESY-F31-86-02.
- [56] M. Pivk and F. R. Le Diberder, *sPlot: A statistical tool to unfold data distributions*, Nucl. Instrum. Meth. **A555** (2005) 356, [arXiv:physics/0402083](https://arxiv.org/abs/physics/0402083).
- [57] J. Back *et al.*, LAURA⁺⁺: *A Dalitz plot fitter*, Comput. Phys. Commun. **231** (2018) 198, [arXiv:1711.09854](https://arxiv.org/abs/1711.09854).
- [58] E. Ben-Haim, R. Brun, B. Echenard, and T. E. Latham, *JFIT: a framework to obtain combined experimental results through joint fits*, [arXiv:1409.5080](https://arxiv.org/abs/1409.5080).
- [59] D. J. Herndon, P. Söding, and R. J. Cashmore, *Generalized isobar model formalism*, Phys. Rev. **D11** (1975) 3165.
- [60] D. Morgan, *Phenomenological analysis of $I = \frac{1}{2}$ single-pion production processes in the energy range 500 to 700 MeV*, Phys. Rev. **166** (1968) 1731.
- [61] G. N. Fleming, *Recoupling effects in the isobar model. I. General formalism for three-pion scattering*, Phys. Rev. **135** (1964) B551.
- [62] D. Aston *et al.*, *A study of $K^-\pi^+$ scattering in the reaction $K^-p \rightarrow K^-\pi^+n$ at 11 GeV/c*, Nucl. Phys. **B296** (1988) 493.
- [63] F. James, *Statistical methods in experimental physics*, World Scientific Publishing (2006).
- [64] LHCb collaboration, R. Aaij *et al.*, *Amplitude analysis of $B^0 \rightarrow \bar{D}^0 D_s^+ \pi^-$ and $B^+ \rightarrow D^- D_s^+ \pi^+$ decays*, Phys. Rev. **D108** (2023) 012017, [arXiv:2212.02717](https://arxiv.org/abs/2212.02717).
- [65] LHCb collaboration, R. Aaij *et al.*, *Evidence of a $J/\psi K_S^0$ structure in $B^0 \rightarrow J/\psi \phi K_S^0$ decays*, Phys. Rev. Lett. **131** (2023) 131901, [arXiv:2301.04899](https://arxiv.org/abs/2301.04899).
- [66] LHCb collaboration, R. Aaij *et al.*, *Observation of the resonant character of the $Z(4430)^-$ state*, Phys. Rev. Lett. **112** (2014) 222002, [arXiv:1404.1903](https://arxiv.org/abs/1404.1903).

LHCb collaboration

R. Aaij³⁸ , A.S.W. Abdelmotteleb⁵⁷ , C. Abellan Beteta⁵¹ , F. Abudinén⁵⁷ , T. Ackernley⁶¹ , A. A. Adefisoye⁶⁹ , B. Adeva⁴⁷ , M. Adinolfi⁵⁵ , P. Adlarson⁸⁵ , C. Agapopoulou¹⁴ , C.A. Aidala⁸⁷ , Z. Ajaltouni¹¹ , S. Akar¹¹ , K. Akiba³⁸ , P. Albicocco²⁸ , J. Albrecht^{19,g} , R. Aleksiejunas⁸⁰ , F. Alessio⁴⁹ , P. Alvarez Cartelle⁵⁶ , R. Amalric¹⁶ , S. Amato³ , J.L. Amey⁵⁵ , Y. Amhis¹⁴ , L. An⁶ , L. Anderlini²⁷ , M. Andersson⁵¹ , P. Andreola⁵¹ , M. Andreotti²⁶ , S. Andres Estrada⁸⁴ , A. Anelli^{31,p,49} , D. Ao⁷ , C. Arata¹² , F. Archilli^{37,w} , Z. Areg⁶⁹ , M. Argenton²⁶ , S. Arguedas Cuendis^{9,49} , L. Arnone^{31,p} , A. Artamonov⁴⁴ , M. Artuso⁶⁹ , E. Aslanides¹³ , R. Ataíde Da Silva⁵⁰ , M. Atzeni⁶⁵ , B. Audurier¹² , J. A. Authier¹⁵ , D. Bacher⁶⁴ , I. Bachiller Perea⁵⁰ , S. Bachmann²² , M. Bachmayer⁵⁰ , J.J. Back⁵⁷ , P. Baladron Rodriguez⁴⁷ , V. Balagura¹⁵ , A. Balboni²⁶ , W. Baldini²⁶ , Z. Baldwin⁷⁸ , L. Balzani¹⁹ , H. Bao⁷ , J. Baptista de Souza Leite² , C. Barbero Pretel^{47,12} , M. Barbetti²⁷ , I. R. Barbosa⁷⁰ , R.J. Barlow⁶³ , M. Barnyakov²⁵ , S. Barsuk¹⁴ , W. Barter⁵⁹ , J. Bartz⁶⁹ , S. Bashir⁴⁰ , B. Batsukh⁵ , P. B. Battista¹⁴ , A. Bay⁵⁰ , A. Beck⁶⁵ , M. Becker¹⁹ , F. Bedeschchi³⁵ , I.B. Bediaga² , N. A. Behling¹⁹ , S. Belin⁴⁷ , A. Bellavista²⁵ , K. Belous⁴⁴ , I. Belov²⁹ , I. Belyaev³⁶ , G. Benane¹³ , G. Bencivenni²⁸ , E. Ben-Haim¹⁶ , A. Berezhnoy⁴⁴ , R. Bernet⁵¹ , S. Bernet Andres⁴⁶ , A. Bertolin³³ , C. Betancourt⁵¹ , F. Betti⁵⁹ , J. Bex⁵⁶ , Ia. Bezshyiko⁵¹ , O. Bezshykyo⁸⁶ , J. Bhom⁴¹ , M.S. Bieker¹⁸ , N.V. Biesuz²⁶ , P. Billoir¹⁶ , A. Biolchini³⁸ , M. Birch⁶² , F.C.R. Bishop¹⁰ , A. Bitadze⁶³ , A. Bizzeti^{27,q} , T. Blake^{57,c} , F. Blanc⁵⁰ , J.E. Blank¹⁹ , S. Blusk⁶⁹ , V. Bocharnikov⁴⁴ , J.A. Boelhauve¹⁹ , O. Boente Garcia¹⁵ , T. Boettcher⁶⁸ , A. Bohare⁵⁹ , A. Boldyrev⁴⁴ , C.S. Bolognani⁸² , R. Bolzonella^{26,m} , R. B. Bonacci¹ , N. Bondar^{44,49} , A. Bordelius⁴⁹ , F. Borgato^{33,49} , S. Borghi⁶³ , M. Borsato^{31,p} , J.T. Borsuk⁸³ , E. Bottalico⁶¹ , S.A. Bouchiba⁵⁰ , M. Bovill⁶⁴ , T.J.V. Bowcock⁶¹ , A. Boyer⁴⁹ , C. Bozzi²⁶ , J. D. Brandenburg⁸⁸ , A. Brea Rodriguez⁵⁰ , N. Breer¹⁹ , J. Brodzicka⁴¹ , A. Brossa Gonzalo^{47,†} , J. Brown⁶¹ , D. Brundu³² , E. Buchanan⁵⁹ , M. Burgos Marcos⁸² , A.T. Burke⁶³ , C. Burr⁴⁹ , C. Buti²⁷ , J.S. Butter⁵⁶ , J. Buytaert⁴⁹ , W. Byczynski⁴⁹ , S. Cadeddu³² , H. Cai⁷⁵ , Y. Cai⁵ , A. Caillet¹⁶ , R. Calabrese^{26,m} , S. Calderon Ramirez⁹ , L. Calefice⁴⁵ , S. Cali²⁸ , M. Calvi^{31,p} , M. Calvo Gomez⁴⁶ , P. Camargo Magalhaes^{2,a} , J. I. Cambon Bouzas⁴⁷ , P. Campana²⁸ , D.H. Campora Perez⁸² , A.F. Campoverde Quezada⁷ , S. Capelli³¹ , M. Caporale²⁵ , L. Capriotti²⁶ , R. Caravaca-Mora⁹ , A. Carbone^{25,k} , L. Carcedo Salgado⁴⁷ , R. Cardinale^{29,n} , A. Cardini³² , P. Carniti³¹ , L. Carus²² , A. Casais Vidal⁶⁵ , R. Caspary²² , G. Casse⁶¹ , M. Cattaneo⁴⁹ , G. Cavallero²⁶ , V. Cavallini^{26,m} , S. Celani²² , I. Celestino^{35,t} , S. Cesare^{30,o} , F. Cesario Laterza Lopes² , A.J. Chadwick⁶¹ , I. Chahroud⁸⁷ , H. Chang^{4,d} , M. Charles¹⁶ , Ph. Charpentier⁴⁹ , E. Chatzianagnostou³⁸ , R. Cheaib⁷⁹ , M. Chefdeville¹⁰ , C. Chen⁵⁶ , J. Chen⁵⁰ , S. Chen⁵ , Z. Chen⁷ , M. Cherif¹² , A. Chernov⁴¹ , S. Chernyshenko⁵³ , X. Chiotopoulos⁸² , V. Chobanova⁸⁴ , M. Chrzaszcz⁴¹ , A. Chubykin⁴⁴ , V. Chulikov^{28,36,49} , P. Ciambrone²⁸ , X. Cid Vidal⁴⁷ , G. Ciezarek⁴⁹ , P. Cifra³⁸ , P.E.L. Clarke⁵⁹ , M. Clemencic⁴⁹ , H.V. Cliff⁵⁶ , J. Closier⁴⁹ , C. Cocha Toapaxi²² , V. Coco⁴⁹ , J. Cogan¹³ , E. Cogneras¹¹ , L. Cojocariu⁴³ , S. Collaviti⁵⁰ , P. Collins⁴⁹ , T. Colombo⁴⁹ , M. Colonna¹⁹ , A. Comerma-Montells⁴⁵ , L. Congedo²⁴ , J. Connaughton⁵⁷ , A. Contu³² , N. Cooke⁶⁰ , G. Cordova^{35,t} , C. Coronel⁶⁶ , I. Corredoira¹² , A. Correia¹⁶ , G. Corti⁴⁹ , J. Cottee Meldrum⁵⁵ , B. Couturier⁴⁹ , D.C. Craik⁵¹ , M. Cruz Torres^{2,h} , E. Curras Rivera⁵⁰ , R. Currie⁵⁹ , C.L. Da Silva⁶⁸ , S. Dadabaev⁴⁴ , L. Dai⁷² , X. Dai⁴ , E. Dall'Occo⁴⁹ , J. Dalseno⁸⁴ , C. D'Ambrosio⁶²

J. Daniel¹¹ , P. d'Argent²⁴ , G. Darze³ , A. Davidson⁵⁷ , J.E. Davies⁶³ , O. De Aguiar Francisco⁶³ , C. De Angelis^{32,l} , F. De Benedetti⁴⁹ , J. de Boer³⁸ , K. De Bruyn⁸¹ , S. De Capua⁶³ , M. De Cian⁶³ , U. De Freitas Carneiro Da Graca^{2,b} , E. De Lucia²⁸ , J.M. De Miranda² , L. De Paula³ , M. De Serio^{24,i} , P. De Simone²⁸ , F. De Vellis¹⁹ , J.A. de Vries⁸² , F. Debernardis²⁴ , D. Decamp¹⁰ , S. Dekkers¹ , L. Del Buono¹⁶ , B. Delaney⁶⁵ , H.-P. Dembinski¹⁹ , J. Deng⁸ , V. Denysenko⁵¹ , O. Deschamps¹¹ , F. Dettori^{32,l} , B. Dey⁷⁹ , P. Di Nezza²⁸ , I. Diachkov⁴⁴ , S. Didenko⁴⁴ , S. Ding⁶⁹ , Y. Ding⁵⁰ , L. Dittmann²² , V. Dobishuk⁵³ , A. D. Docheva⁶⁰ , A. Doheny⁵⁷ , C. Dong^{4,d} , A.M. Donohoe²³ , F. Dordei³² , A.C. dos Reis² , A. D. Dowling⁶⁹ , L. Dreyfus¹³ , W. Duan⁷³ , P. Duda⁸³ , L. Dufour⁴⁹ , V. Duk³⁴ , P. Durante⁴⁹ , M. M. Duras⁸³ , J.M. Durham⁶⁸ , O. D. Durmus⁷⁹ , A. Dziurda⁴¹ , A. Dzyuba⁴⁴ , S. Easo⁵⁸ , E. Eckstein¹⁸ , U. Egede¹ , A. Egorychev⁴⁴ , V. Egorychev⁴⁴ , S. Eisenhardt⁵⁹ , E. Ejopu⁶¹ , L. Eklund⁸⁵ , M. Elashri⁶⁶ , J. Ellbracht¹⁹ , S. Ely⁶² , A. Ene⁴³ , J. Eschle⁶⁹ , S. Esen²² , T. Evans³⁸ , F. Fabiano³² , S. Faghih⁶⁶ , L.N. Falcao² , B. Fang⁷ , R. Fantechi³⁵ , L. Fantini^{34,s} , M. Faria⁵⁰ , K. Farmer⁵⁹ , D. Fazzini^{31,p} , L. Felkowski⁸³ , M. Feng^{5,7} , M. Feo¹⁹ , A. Fernandez Casani⁴⁸ , M. Fernandez Gomez⁴⁷ , A.D. Fernez⁶⁷ , F. Ferrari^{25,k} , F. Ferreira Rodrigues³ , M. Ferrillo⁵¹ , M. Ferro-Luzzi⁴⁹ , S. Filippov⁴⁴ , R.A. Fini²⁴ , M. Fiorini^{26,m} , M. Firlej⁴⁰ , K.L. Fischer⁶⁴ , D.S. Fitzgerald⁸⁷ , C. Fitzpatrick⁶³ , T. Fiutowski⁴⁰ , F. Fleuret¹⁵ , A. Fomin⁵² , M. Fontana²⁵ , L. F. Foreman⁶³ , R. Forty⁴⁹ , D. Foulds-Holt⁵⁹ , V. Franco Lima³ , M. Franco Sevilla⁶⁷ , M. Frank⁴⁹ , E. Franzoso^{26,m} , G. Frau⁶³ , C. Frei⁴⁹ , D.A. Friday^{63,49} , J. Fu⁷ , Q. Führing^{19,g,56} , T. Fulghesu¹³ , G. Galati²⁴ , M.D. Galati³⁸ , A. Gallas Torreira⁴⁷ , D. Galli^{25,k} , S. Gambetta⁵⁹ , M. Gandelman³ , P. Gandini³⁰ , B. Ganie⁶³ , H. Gao⁷ , R. Gao⁶⁴ , T.Q. Gao⁵⁶ , Y. Gao⁸ , Y. Gao⁶ , Y. Gao⁸ , L.M. Garcia Martin⁵⁰ , P. Garcia Moreno⁴⁵ , J. García Pardiñas⁶⁵ , P. Gardner⁶⁷ , K. G. Garg⁸ , L. Garrido⁴⁵ , C. Gaspar⁴⁹ , A. Gavrikov³³ , L.L. Gerken¹⁹ , E. Gersabeck²⁰ , M. Gersabeck²⁰ , T. Gershon⁵⁷ , S. Ghizzo^{29,n} , Z. Ghorbanimoghaddam⁵⁵ , L. Giambastiani^{33,r} , F. I. Giasemis^{16,f} , V. Gibson⁵⁶ , H.K. Giemza⁴² , A.L. Gilman⁶⁴ , M. Giovannetti²⁸ , A. Gioventù⁴⁵ , L. Girardey^{63,58} , M.A. Giza⁴¹ , F.C. Glaser^{14,22} , V.V. Gligorov¹⁶ , C. Göbel⁷⁰ , L. Golinka-Bezshyyko⁸⁶ , E. Golobardes⁴⁶ , D. Golubkov⁴⁴ , A. Golutvin^{62,49} , S. Gomez Fernandez⁴⁵ , W. Gomulka⁴⁰ , I. Gonçales Vaz⁴⁹ , F. Goncalves Abrantes⁶⁴ , M. Goncerz⁴¹ , G. Gong^{4,d} , J. A. Gooding¹⁹ , I.V. Gorelov⁴⁴ , C. Gotti³¹ , E. Govorkova⁶⁵ , J.P. Grabowski¹⁸ , L.A. Granado Cardoso⁴⁹ , E. Graugés⁴⁵ , E. Graverini^{50,u} , L. Grazette⁵⁷ , G. Graziani²⁷ , A. T. Grecu⁴³ , L.M. Greeven³⁸ , N.A. Grieser⁶⁶ , L. Grillo⁶⁰ , S. Gromov⁴⁴ , C. Gu¹⁵ , M. Guarise²⁶ , L. Guerry¹¹ , V. Guliaeva⁴⁴ , P. A. Günther²² , A.-K. Guseinov⁵⁰ , E. Gushchin⁴⁴ , Y. Guz^{6,49} , T. Gys⁴⁹ , K. Habermann¹⁸ , T. Hadavizadeh¹ , C. Hadjivasiliou⁶⁷ , G. Haefeli⁵⁰ , C. Haen⁴⁹ , S. Haken⁵⁶ , G. Hallett⁵⁷ , P.M. Hamilton⁶⁷ , J. Hammerich⁶¹ , Q. Han³³ , X. Han^{22,49} , S. Hansmann-Menzemer²² , L. Hao⁷ , N. Harnew⁶⁴ , T. H. Harris¹ , M. Hartmann¹⁴ , S. Hashmi⁴⁰ , J. He^{7,e} , A. Hedes⁶³ , F. Hemmer⁴⁹ , C. Henderson⁶⁶ , R. Henderson¹⁴ , R.D.L. Henderson¹ , A.M. Hennequin⁴⁹ , K. Hennessy⁶¹ , L. Henry⁵⁰ , J. Herd⁶² , P. Herrero Gascon²² , J. Heuel¹⁷ , A. Hicheur³ , G. Hijano Mendizabal⁵¹ , J. Horswill⁶³ , R. Hou⁸ , Y. Hou¹¹ , D. C. Houston⁶⁰ , N. Howarth⁶¹ , J. Hu⁷³ , W. Hu⁷ , X. Hu^{4,d} , W. Hulsbergen³⁸ , R.J. Hunter⁵⁷ , M. Hushchyn⁴⁴ , D. Hutchcroft⁶¹ , M. Idzik⁴⁰ , D. Ilin⁴⁴ , P. Ilten⁶⁶ , A. Iniukhin⁴⁴ , A. Iohner¹⁰ , A. Ishteev⁴⁴ , K. Ivshin⁴⁴ , H. Jage¹⁷ , S.J. Jaimes Elles^{77,48,49} , S. Jakobsen⁴⁹ , E. Jans³⁸ , B.K. Jashal⁴⁸ , A. Jawahery⁶⁷ , C. Jayaweera⁵⁴ , V. Jevtic¹⁹ , Z. Jia¹⁶ , E. Jiang⁶⁷ , X. Jiang^{5,7} , Y. Jiang⁷ , Y. J.

Jiang⁶ , E. Jimenez Moya⁹ , N. Jindal⁸⁸ , M. John⁶⁴ , A. John Rubesh Rajan²³ , D. Johnson⁵⁴ , C.R. Jones⁵⁶ , S. Joshi⁴² , B. Jost⁴⁹ , J. Juan Castella⁵⁶ , N. Jurik⁴⁹ , I. Juszczak⁴¹ , D. Kaminaris⁵⁰ , S. Kandybei⁵² , M. Kane⁵⁹ , Y. Kang^{4,d} , C. Kar¹¹ , M. Karacson⁴⁹ , A. Kauniskangas⁵⁰ , J.W. Kautz⁶⁶ , M.K. Kazanecki⁴¹ , F. Keizer⁴⁹ , M. Kenzie⁵⁶ , T. Ketel³⁸ , B. Khanji⁶⁹ , A. Kharisova⁴⁴ , S. Kholodenko^{62,49} , G. Khreich¹⁴ , T. Kirn¹⁷ , V.S. Kirsebom^{31,p} , O. Kitouni⁶⁵ , S. Klaver³⁹ , N. Kleijne^{35,t} , D. K. Klekots⁸⁶ , K. Klimaszewski⁴² , M.R. Kmiec⁴² , T. Knospe¹⁹ , S. Koliiev⁵³ , L. Kolk¹⁹ , A. Konoplyannikov⁶ , P. Kopciewicz⁴⁹ , P. Koppenburg³⁸ , A. Korchin⁵² , M. Korolev⁴⁴ , I. Kostiuk³⁸ , O. Kot⁵³ , S. Kotriakhova , E. Kowalczyk⁶⁷ , A. Kozachuk⁴⁴ , P. Kravchenko⁴⁴ , L. Kravchuk⁴⁴ , O. Kravcov⁸⁰ , M. Kreps⁵⁷ , P. Krokovny⁴⁴ , W. Krupa⁶⁹ , W. Krzemien⁴² , O. Kshyvanskyi⁵³ , S. Kubis⁸³ , M. Kucharczyk⁴¹ , V. Kudryavtsev⁴⁴ , E. Kulikova⁴⁴ , A. Kups⁸⁵ , V. Kushnir⁵² , B. Kutsenko¹³ , J. Kvapil⁶⁸ , I. Kyryllin⁵² , D. Lacarrere⁴⁹ , P. Laguarta Gonzalez⁴⁵ , A. Lai³² , A. Lampis³² , D. Lancierini⁶² , C. Landesa Gomez⁴⁷ , J.J. Lane¹ , G. Lanfranchi²⁸ , C. Langenbruch²² , J. Langer¹⁹ , O. Lantwin⁴⁴ , T. Latham⁵⁷ , F. Lazzari^{35,u,49} , C. Lazzeroni⁵⁴ , R. Le Gac¹³ , H. Lee⁶¹ , R. Lefevre¹¹ , A. Leflat⁴⁴ , S. Legotin⁴⁴ , M. Lehuraux⁵⁷ , E. Lemos Cid⁴⁹ , O. Leroy¹³ , T. Lesiak⁴¹ , E. D. Lesser⁴⁹ , B. Leverington²² , A. Li^{4,d} , C. Li⁴ , C. Li¹³ , H. Li⁷³ , J. Li⁸ , K. Li⁷⁶ , L. Li⁶³ , M. Li⁸ , P. Li⁷ , P.-R. Li⁷⁴ , Q. Li^{5,7} , T. Li⁷² , T. Li⁷³ , Y. Li⁸ , Y. Li⁵ , Y. Li⁴ , Z. Lian^{4,d} , Q. Liang⁸ , X. Liang⁶⁹ , Z. Liang³² , S. Libralon⁴⁸ , A. L. Lightbody¹² , C. Lin⁷ , T. Lin⁵⁸ , R. Lindner⁴⁹ , H. Linton⁶² , R. Litvinov³² , D. Liu⁸ , F. L. Liu¹ , G. Liu⁷³ , K. Liu⁷⁴ , S. Liu^{5,7} , W. Liu⁸ , Y. Liu⁵⁹ , Y. Liu⁷⁴ , Y. L. Liu⁶² , G. Loachamin Ordóñez⁷⁰ , A. Lobo Salvia⁴⁵ , A. Loi³² , T. Long⁵⁶ , J.H. Lopes³ , A. Lopez Huertas⁴⁵ , C. Lopez Iribarne⁴⁷ , S. López Soliño⁴⁷ , Q. Lu¹⁵ , C. Lucarelli⁴⁹ , D. Lucchesi^{33,r} , M. Lucio Martinez⁴⁸ , Y. Luo⁶ , A. Lupato^{33,j} , E. Luppi^{26,m} , K. Lynch²³ , X.-R. Lyu⁷ , G. M. Ma^{4,d} , S. Maccolini¹⁹ , F. Machefert¹⁴ , F. Maciuc⁴³ , B. Mack⁶⁹ , I. Mackay⁶⁴ , L.M. Mackey⁶⁹ , L.R. Madhan Mohan⁵⁶ , M. J. Madurai⁵⁴ , D. Magdalinski³⁸ , D. Maisuzenko⁴⁴ , J.J. Malczewski⁴¹ , S. Malde⁶⁴ , L. Malentacca⁴⁹ , A. Malinin⁴⁴ , T. Maltsev⁴⁴ , G. Manca^{32,l} , G. Mancinelli¹³ , C. Mancuso¹⁴ , R. Manera Escalero⁴⁵ , F. M. Manganella³⁷ , D. Manuzzi²⁵ , D. Marangotto^{30,o} , J.F. Marchand¹⁰ , R. Marchevski⁵⁰ , U. Marconi²⁵ , E. Mariani¹⁶ , S. Mariani⁴⁹ , C. Marin Benito⁴⁵ , J. Marks²² , A.M. Marshall⁵⁵ , L. Martel⁶⁴ , G. Martelli³⁴ , G. Martellotti³⁶ , L. Martinazzoli⁴⁹ , M. Martinelli^{31,p} , D. Martinez Gomez⁸¹ , D. Martinez Santos⁸⁴ , F. Martinez Vidal⁴⁸ , A. Martorell i Granollers⁴⁶ , A. Massafferri² , R. Matev⁴⁹ , A. Mathad⁴⁹ , V. Matiunin⁴⁴ , C. Matteuzzi⁶⁹ , K.R. Mattioli¹⁵ , A. Mauri⁶² , E. Maurice¹⁵ , J. Mauricio⁴⁵ , P. Mayencourt⁵⁰ , J. Mazorra de Cos⁴⁸ , M. Mazurek⁴² , M. McCann⁶² , T.H. McGrath⁶³ , N.T. McHugh⁶⁰ , A. McNab⁶³ , R. McNulty²³ , B. Meadows⁶⁶ , G. Meier¹⁹ , D. Melnychuk⁴² , D. Mendoza Granada¹⁶ , P. Menendez Valdes Perez⁴⁷ , F. Meng^{4,d} , M. Merk^{38,82} , A. Merli^{50,30} , L. Meyer Garcia⁶⁷ , D. Miao^{5,7} , H. Miao⁷ , M. Mikhasenko⁷⁸ , D.A. Milanes^{77,z} , A. Minott^{31,p} , E. Minucci²⁸ , T. Miralles¹¹ , B. Mitreska¹⁹ , D.S. Mitzel¹⁹ , A. Modak⁵⁸ , L. Moeser¹⁹ , R.D. Moise¹⁷ , E. F. Molina Cardenas⁸⁷ , T. Mombächer⁴⁹ , M. Monk^{57,1} , S. Monteil¹¹ , A. Morcillo Gomez⁴⁷ , G. Morello²⁸ , M.J. Morello^{35,t} , M.P. Morgenthaler²² , A. Moro^{31,p} , J. Moron⁴⁰ , W. Morren³⁸ , A.B. Morris⁴⁹ , A.G. Morris¹³ , R. Mountain⁶⁹ , H. Mu^{4,d} , Z. M. Mu⁶ , E. Muhammad⁵⁷ , F. Muheim⁵⁹ , M. Mulder⁸¹ , K. Müller⁵¹ , F. Muñoz-Rojas⁹ , R. Murta⁶² , V. Mytrochenko⁵² , P. Naik⁶¹ , T. Nakada⁵⁰ , R. Nandakumar⁵⁸ , T. Nanut⁴⁹ , I. Nasteva³ , M. Needham⁵⁹ , E. Nekrasova⁴⁴ , N. Neri^{30,o} , S. Neubert¹⁸

N. Neufeld⁴⁹ , P. Neustroev⁴⁴, J. Nicolini⁴⁹ , D. Nicotra⁸² , E.M. Niel¹⁵ , N. Nikitin⁴⁴ ,
 L. Nisi¹⁹ , Q. Niu⁷⁴ , P. Nogarolli³ , P. Nogga¹⁸ , C. Normand⁵⁵ ,
 J. Novoa Fernandez⁴⁷ , G. Nowak⁶⁶ , C. Nunez⁸⁷ , H. N. Nur⁶⁰ ,
 A. Oblakowska-Mucha⁴⁰ , V. Obraztsov⁴⁴ , T. Oeser¹⁷ , A. Okhotnikov⁴⁴,
 O. Okhrimenko⁵³ , R. Oldeman^{32,l} , F. Oliva^{59,49} , E. Olivart Pino⁴⁵ , M. Olocco¹⁹ ,
 C.J.G. Onderwater⁸² , R.H. O'Neil⁴⁹ , J.S. Ordonez Soto¹¹ , D. Osthuus¹⁹ ,
 J.M. Otalora Goicochea³ , P. Owen⁵¹ , A. Oyanguren⁴⁸ , O. Ozcelik⁴⁹ , F. Paciolla^{35,x} ,
 A. Padde⁴² , K.O. Padeken¹⁸ , B. Pagare⁴⁷ , T. Pajero⁴⁹ , A. Palano²⁴ ,
 M. Palutan²⁸ , C. Pan⁷⁵ , X. Pan^{4,d} , S. Panebianco¹² , G. Panshin⁵ ,
 L. Paolucci⁶³ , A. Papanestis⁵⁸ , M. Pappagallo^{24,i} , L.L. Pappalardo²⁶ ,
 C. Pappenheimer⁶⁶ , C. Parkes⁶³ , D. Parmar⁷⁸ , B. Passalacqua^{26,m} , G. Passaleva²⁷ ,
 D. Passaro^{35,t,49} , A. Pastore²⁴ , M. Patel⁶² , J. Patoc⁶⁴ , C. Patrignani^{25,k} , A. Paul⁶⁹ , C.J. Pawley⁸² , A. Pellegrino³⁸ , J. Peng^{5,7} , X. Peng⁷⁴, M. Pepe Altarelli²⁸ ,
 S. Perazzini²⁵ , D. Pereima⁴⁴ , H. Pereira Da Costa⁶⁸ , M. Pereira Martinez⁴⁷ ,
 A. Pereiro Castro⁴⁷ , C. Perez⁴⁶ , P. Perret¹¹ , A. Perrevoort⁸¹ , A. Perro^{49,13} ,
 M.J. Peters⁶⁶ , K. Petridis⁵⁵ , A. Petrolini^{29,n} , S. Pezzulo^{29,n} , J. P. Pfaller⁶⁶ ,
 H. Pham⁶⁹ , L. Pica^{35,t} , M. Piccini³⁴ , L. Piccolo³² , B. Pietrzek¹⁰ , G. Pietrzek¹⁴ ,
 R. N. Pilato⁶¹ , D. Pinci³⁶ , F. Pisani⁴⁹ , M. Pizzichemi^{31,p,49} , V. M. Placinta⁴³ ,
 M. Plo Casasus⁴⁷ , T. Poeschl⁴⁹ , F. Polci¹⁶ , M. Poli Lener²⁸ , A. Poluektov¹³ ,
 N. Polukhina⁴⁴ , I. Polyakov⁶³ , E. Polycarpo³ , S. Ponce⁴⁹ , D. Popov^{7,49} ,
 S. Poslavskii⁴⁴ , K. Prasant⁵⁹ , C. Prouve⁸⁴ , D. Provenzano^{32,l,49} , V. Pugatch⁵³ ,
 G. Punzi^{35,u} , J.R. Pybus⁶⁸ , S. Qasim⁵¹ , Q. Q. Qian⁶ , W. Qian⁷ , N. Qin^{4,d} ,
 S. Qu^{4,d} , R. Quagliani⁴⁹ , R.I. Rabadan Trejo⁵⁷ , R. Racz⁸⁰ , J.H. Rademacker⁵⁵ ,
 M. Rama³⁵ , M. Ramírez García⁸⁷ , V. Ramos De Oliveira⁷⁰ , M. Ramos Pernas⁵⁷ ,
 M.S. Rangel³ , F. Ratnikov⁴⁴ , G. Raven³⁹ , M. Rebollo De Miguel⁴⁸ , F. Redi^{30,j} ,
 J. Reich⁵⁵ , F. Reiss²⁰ , Z. Ren⁷ , P.K. Resmi⁶⁴ , M. Ribalda Galvez⁴⁵ ,
 R. Ribatti⁵⁰ , G. Ricart^{15,12} , D. Riccardi^{35,t} , S. Ricciardi⁵⁸ , K. Richardson⁶⁵ ,
 M. Richardson-Slipper⁵⁶ , K. Rinnert⁶¹ , P. Robbe^{14,49} , G. Robertson⁶⁰ ,
 E. Rodrigues⁶¹ , A. Rodriguez Alvarez⁴⁵ , E. Rodriguez Fernandez⁴⁷ ,
 J.A. Rodriguez Lopez⁷⁷ , E. Rodriguez Rodriguez⁴⁹ , J. Roensch¹⁹ , A. Rogachev⁴⁴ ,
 A. Rogovskiy⁵⁸ , D.L. Rolf¹⁹ , P. Roloff⁴⁹ , V. Romanovskiy⁶⁶ , A. Romero Vidal⁴⁷ ,
 G. Romolini^{26,49} , F. Ronchetti⁵⁰ , T. Rong⁶ , M. Rotondo²⁸ , S. R. Roy²² ,
 M.S. Rudolph⁶⁹ , M. Ruiz Diaz²² , R.A. Ruiz Fernandez⁴⁷ , J. Ruiz Vidal⁸² , J.
 J. Saavedra-Arias⁹ , J.J. Saborido Silva⁴⁷ , S. E. R. Sacha Emile R.⁴⁹ , N. Sagidova⁴⁴ ,
 D. Sahoo⁷⁹ , N. Sahoo⁵⁴ , B. Saitta^{32,l} , M. Salomoni^{31,49,p} , I. Sanderswood⁴⁸ ,
 R. Santacesaria³⁶ , C. Santamarina Rios⁴⁷ , M. Santimaria²⁸ , L. Santoro² ,
 E. Santovetti³⁷ , A. Saputi^{26,49} , D. Saranin⁴⁴ , A. Sarnatskiy⁸¹ , G. Sarpis⁴⁹ ,
 M. Sarpis⁸⁰ , C. Satriano^{36,v} , A. Satta³⁷ , M. Saur⁷⁴ , D. Savrina⁴⁴ , H. Sazak¹⁷ ,
 F. Sborzacchi^{49,28} , A. Scarabotto¹⁹ , S. Schael¹⁷ , S. Scherl⁶¹ , M. Schiller²² ,
 H. Schindler⁴⁹ , M. Schmelling²¹ , B. Schmidt⁴⁹ , N. Schmidt⁶⁸ , S. Schmitt¹⁷ ,
 H. Schmitz¹⁸, O. Schneider⁵⁰ , A. Schopper⁶² , N. Schulte¹⁹ , M.H. Schunke¹⁴ ,
 G. Schwering¹⁷ , B. Sciascia²⁸ , A. Sciuccati⁴⁹ , G. Scriven⁸² , I. Segal⁷⁸ ,
 S. Sellam⁴⁷ , A. Semennikov⁴⁴ , T. Senger⁵¹ , M. Senghi Soares³⁹ , A. Sergi^{29,n,49} ,
 N. Serra⁵¹ , L. Sestini²⁷ , A. Seuthe¹⁹ , B. Sevilla Sanjuan⁴⁶ , Y. Shang⁶ ,
 D.M. Shangase⁸⁷ , M. Shapkin⁴⁴ , R. S. Sharma⁶⁹ , I. Shchemerov⁴⁴ , L. Shchutska⁵⁰ ,
 T. Shears⁶¹ , L. Shekhtman⁴⁴ , Z. Shen³⁸ , S. Sheng^{5,7} , V. Shevchenko⁴⁴ , B. Shi⁷ ,
 Q. Shi⁷ , W. S. Shi⁷³ , Y. Shimizu¹⁴ , E. Shmanin²⁵ , R. Shorkin⁴⁴ ,
 J.D. Shupperd⁶⁹ , R. Silva Coutinho⁶⁹ , G. Simi^{33,r} , S. Simone^{24,i} , M. Singha⁷⁹ ,
 N. Skidmore⁵⁷ , T. Skwarnicki⁶⁹ , M.W. Slater⁵⁴ , E. Smith⁶⁵ , K. Smith⁶⁸ ,
 M. Smith⁶² , L. Soares Lavra⁵⁹ , M.D. Sokoloff⁶⁶ , F.J.P. Soler⁶⁰ , A. Solomin⁵⁵ 

A. Solovev⁴⁴ , K. Solovieva²⁰ , N. S. Sommerfeld¹⁸ , R. Song¹ , Y. Song⁵⁰ ,
 Y. Song^{4,d} , Y. S. Song⁶ , F.L. Souza De Almeida⁶⁹ , B. Souza De Paula³ , K.M. Sowa⁴⁰,
 E. Spadaro Norella^{29,n} , E. Spedicato²⁵ , J.G. Speer¹⁹ , P. Spradlin⁶⁰ , V. Sriskaran⁴⁹ ,
 F. Stagni⁴⁹ , M. Stahl⁷⁸ , S. Stahl⁴⁹ , S. Stanislaus⁶⁴ , M. Stefaniak⁸⁸ , E.N. Stein⁴⁹ ,
 O. Steinkamp⁵¹ , H. Stevens¹⁹ , D. Strekalina⁴⁴ , Y. Su⁷ , F. Suljik⁶⁴ , J. Sun³² , J.
 Sun⁶³ , L. Sun⁷⁵ , D. Sundfeld² , W. Sutcliffe⁵¹ , V. Svintozelskyi⁴⁸ , K. Swientek⁴⁰ ,
 F. Swystun⁵⁶ , A. Szabelski⁴² , T. Szumlak⁴⁰ , Y. Tan^{4,d} , Y. Tang⁷⁵ , Y. T. Tang⁷ ,
 M.D. Tat²² , J. A. Teijeiro Jimenez⁴⁷ , A. Terentev⁴⁴ , F. Terzuoli^{35,x} , F. Teubert⁴⁹ ,
 E. Thomas⁴⁹ , D.J.D. Thompson⁵⁴ , A. R. Thomson-Strong⁵⁹ , H. Tilquin⁶² ,
 V. Tisserand¹¹ , S. T'Jampens¹⁰ , M. Tobin^{5,49} , T. T. Todorov²⁰ , L. Tomassetti^{26,m} ,
 G. Tonani³⁰ , X. Tong⁶ , T. Tork³⁰ , D. Torres Machado² , L. Toscano¹⁹ ,
 D.Y. Tou^{4,d} , C. Tripli⁴⁶ , G. Tuci²² , N. Tuning³⁸ , L.H. Uecker²² , A. Ukleja⁴⁰ ,
 D.J. Unverzagt²² , A. Upadhyay⁴⁹ , B. Urbach⁵⁹ , A. Usachov³⁹ , A. Ustyuzhanin⁴⁴ ,
 U. Uwer²² , V. Vagnoni²⁵ , V. Valcarce Cadenas⁴⁷ , G. Valenti²⁵ ,
 N. Valls Canudas⁴⁹ , J. van Eldik⁴⁹ , H. Van Hecke⁶⁸ , E. van Herwijnen⁶² ,
 C.B. Van Hulse^{47,aa} , R. Van Laak⁵⁰ , M. van Veghel³⁸ , G. Vasquez⁵¹ ,
 R. Vazquez Gomez⁴⁵ , P. Vazquez Regueiro⁴⁷ , C. Vázquez Sierra⁸⁴ , S. Vecchi²⁶ , J.
 Velilla Serna⁴⁸ , J.J. Velthuis⁵⁵ , M. Veltri^{27,y} , A. Venkateswaran⁵⁰ , M. Verdoglia³² ,
 M. Vesterinen⁵⁷ , W. Vetens⁶⁹ , D. Vico Benet⁶⁴ , P. Vidrier Villalba⁴⁵ ,
 M. Vieites Diaz^{47,49} , X. Vilasis-Cardona⁴⁶ , E. Vilella Figueras⁶¹ , A. Villa²⁵ ,
 P. Vincent¹⁶ , B. Vivacqua³ , F.C. Volle⁵⁴ , D. vom Bruch¹³ , N. Voropaev⁴⁴ ,
 K. Vos⁸² , C. Vrahas⁵⁹ , J. Wagner¹⁹ , J. Walsh³⁵ , E.J. Walton^{1,57} , G. Wan⁶ , A.
 Wang⁷ , B. Wang⁵ , C. Wang²² , G. Wang⁸ , H. Wang⁷⁴ , J. Wang⁶ , J. Wang⁵ ,
 J. Wang^{4,d} , J. Wang⁷⁵ , M. Wang⁴⁹ , N. W. Wang⁷ , R. Wang⁵⁵ , X. Wang⁸ ,
 X. Wang⁷³ , X. W. Wang⁶² , Y. Wang⁷⁶ , Y. Wang⁶ , Y. H. Wang⁷⁴ , Z. Wang¹⁴ ,
 Z. Wang^{4,d} , Z. Wang³⁰ , J.A. Ward⁵⁷ , M. Waterlaat⁴⁹ , N.K. Watson⁵⁴ ,
 D. Websdale⁶² , Y. Wei⁶ , Z. Weida⁷ , J. Wendel⁸⁴ , B.D.C. Westhenry⁵⁵ ,
 C. White⁵⁶ , M. Whitehead⁶⁰ , E. Whiter⁵⁴ , A.R. Wiederhold⁶³ , D. Wiedner¹⁹ , M.
 A. Wiegertjes³⁸ , C. Wild⁶⁴ , G. Wilkinson^{64,49} , M.K. Wilkinson⁶⁶ , M. Williams⁶⁵ ,
 M. J. Williams⁴⁹ , M.R.J. Williams⁵⁹ , R. Williams⁵⁶ , S. Williams⁵⁵ , Z. Williams⁵⁵ ,
 F.F. Wilson⁵⁸ , M. Winn¹² , W. Wislicki⁴² , M. Witek⁴¹ , L. Witola¹⁹ , T. Wolf²² , E.
 Wood⁵⁶ , G. Wormser¹⁴ , S.A. Wotton⁵⁶ , H. Wu⁶⁹ , J. Wu⁸ , X. Wu⁷⁵ , Y. Wu^{6,56} ,
 Z. Wu⁷ , K. Wyllie⁴⁹ , S. Xian⁷³ , Z. Xiang⁵ , Y. Xie⁸ , T. X. Xing³⁰ , A. Xu^{35,t} ,
 L. Xu^{4,d} , L. Xu^{4,d} , M. Xu⁴⁹ , Z. Xu⁴⁹ , Z. Xu⁷ , Z. Xu⁵ , K. Yang⁶² ,
 X. Yang⁶ , Y. Yang¹⁵ , Z. Yang⁶ , V. Yeroshenko¹⁴ , H. Yeung⁶³ , H. Yin⁸ , X.
 Yin⁷ , C. Y. Yu⁶ , J. Yu⁷² , X. Yuan⁵ , Y. Yuan^{5,7} , E. Zaffaroni⁵⁰ , J.
 A. Zamora Saa⁷¹ , M. Zavyalova²¹ , M. Zdybal⁴¹ , F. Zenesini²⁵ , C. Zeng^{5,7} ,
 M. Zeng^{4,d} , C. Zhang⁶ , D. Zhang⁸ , J. Zhang⁷ , L. Zhang^{4,d} , R. Zhang⁸ ,
 S. Zhang⁷² , S. Zhang⁶⁴ , Y. Zhang⁶ , Y. Z. Zhang^{4,d} , Z. Zhang^{4,d} , Y. Zhao²² ,
 A. Zhelezov²² , S. Z. Zheng⁶ , X. Z. Zheng^{4,d} , Y. Zheng⁷ , T. Zhou⁶ , X. Zhou⁸ ,
 Y. Zhou⁷ , V. Zhovkovska⁵⁷ , L. Z. Zhu⁷ , X. Zhu^{4,d} , X. Zhu⁸ , Y. Zhu¹⁷ ,
 V. Zhukov¹⁷ , J. Zhuo⁴⁸ , Q. Zou^{5,7} , D. Zuliani^{33,r} , G. Zunic²⁸ 

¹School of Physics and Astronomy, Monash University, Melbourne, Australia

²Centro Brasileiro de Pesquisas Físicas (CBPF), Rio de Janeiro, Brazil

³Universidade Federal do Rio de Janeiro (UFRJ), Rio de Janeiro, Brazil

⁴Department of Engineering Physics, Tsinghua University, Beijing, China

⁵Institute Of High Energy Physics (IHEP), Beijing, China

⁶School of Physics State Key Laboratory of Nuclear Physics and Technology, Peking University, Beijing, China

⁷University of Chinese Academy of Sciences, Beijing, China

- ⁸*Institute of Particle Physics, Central China Normal University, Wuhan, Hubei, China*
- ⁹*Consejo Nacional de Rectores (CONARE), San Jose, Costa Rica*
- ¹⁰*Université Savoie Mont Blanc, CNRS, IN2P3-LAPP, Annecy, France*
- ¹¹*Université Clermont Auvergne, CNRS/IN2P3, LPC, Clermont-Ferrand, France*
- ¹²*Université Paris-Saclay, Centre d'Etudes de Saclay (CEA), IRFU, Saclay, France, Gif-Sur-Yvette, France*
- ¹³*Aix Marseille Univ, CNRS/IN2P3, CPPM, Marseille, France*
- ¹⁴*Université Paris-Saclay, CNRS/IN2P3, IJCLab, Orsay, France*
- ¹⁵*Laboratoire Leprince-Ringuet, CNRS/IN2P3, Ecole Polytechnique, Institut Polytechnique de Paris, Palaiseau, France*
- ¹⁶*LPNHE, Sorbonne Université, Paris Diderot Sorbonne Paris Cité, CNRS/IN2P3, Paris, France*
- ¹⁷*I. Physikalisches Institut, RWTH Aachen University, Aachen, Germany*
- ¹⁸*Universität Bonn - Helmholtz-Institut für Strahlen und Kernphysik, Bonn, Germany*
- ¹⁹*Fakultät Physik, Technische Universität Dortmund, Dortmund, Germany*
- ²⁰*Physikalischs Institut, Albert-Ludwigs-Universität Freiburg, Freiburg, Germany*
- ²¹*Max-Planck-Institut für Kernphysik (MPIK), Heidelberg, Germany*
- ²²*Physikalischs Institut, Ruprecht-Karls-Universität Heidelberg, Heidelberg, Germany*
- ²³*School of Physics, University College Dublin, Dublin, Ireland*
- ²⁴*INFN Sezione di Bari, Bari, Italy*
- ²⁵*INFN Sezione di Bologna, Bologna, Italy*
- ²⁶*INFN Sezione di Ferrara, Ferrara, Italy*
- ²⁷*INFN Sezione di Firenze, Firenze, Italy*
- ²⁸*INFN Laboratori Nazionali di Frascati, Frascati, Italy*
- ²⁹*INFN Sezione di Genova, Genova, Italy*
- ³⁰*INFN Sezione di Milano, Milano, Italy*
- ³¹*INFN Sezione di Milano-Bicocca, Milano, Italy*
- ³²*INFN Sezione di Cagliari, Monserrato, Italy*
- ³³*INFN Sezione di Padova, Padova, Italy*
- ³⁴*INFN Sezione di Perugia, Perugia, Italy*
- ³⁵*INFN Sezione di Pisa, Pisa, Italy*
- ³⁶*INFN Sezione di Roma La Sapienza, Roma, Italy*
- ³⁷*INFN Sezione di Roma Tor Vergata, Roma, Italy*
- ³⁸*Nikhef National Institute for Subatomic Physics, Amsterdam, Netherlands*
- ³⁹*Nikhef National Institute for Subatomic Physics and VU University Amsterdam, Amsterdam, Netherlands*
- ⁴⁰*AGH - University of Krakow, Faculty of Physics and Applied Computer Science, Kraków, Poland*
- ⁴¹*Henryk Niewodniczanski Institute of Nuclear Physics Polish Academy of Sciences, Kraków, Poland*
- ⁴²*National Center for Nuclear Research (NCBJ), Warsaw, Poland*
- ⁴³*Horia Hulubei National Institute of Physics and Nuclear Engineering, Bucharest-Magurele, Romania*
- ⁴⁴*Authors affiliated with an institute formerly covered by a cooperation agreement with CERN.*
- ⁴⁵*ICCUB, Universitat de Barcelona, Barcelona, Spain*
- ⁴⁶*La Salle, Universitat Ramon Llull, Barcelona, Spain*
- ⁴⁷*Instituto Galego de Física de Altas Enerxías (IGFAE), Universidade de Santiago de Compostela, Santiago de Compostela, Spain*
- ⁴⁸*Instituto de Fisica Corpuscular, Centro Mixto Universidad de Valencia - CSIC, Valencia, Spain*
- ⁴⁹*European Organization for Nuclear Research (CERN), Geneva, Switzerland*
- ⁵⁰*Institute of Physics, Ecole Polytechnique Fédérale de Lausanne (EPFL), Lausanne, Switzerland*
- ⁵¹*Physik-Institut, Universität Zürich, Zürich, Switzerland*
- ⁵²*NSC Kharkiv Institute of Physics and Technology (NSC KIPT), Kharkiv, Ukraine*
- ⁵³*Institute for Nuclear Research of the National Academy of Sciences (KINR), Kyiv, Ukraine*
- ⁵⁴*School of Physics and Astronomy, University of Birmingham, Birmingham, United Kingdom*
- ⁵⁵*H.H. Wills Physics Laboratory, University of Bristol, Bristol, United Kingdom*
- ⁵⁶*Cavendish Laboratory, University of Cambridge, Cambridge, United Kingdom*
- ⁵⁷*Department of Physics, University of Warwick, Coventry, United Kingdom*
- ⁵⁸*STFC Rutherford Appleton Laboratory, Didcot, United Kingdom*
- ⁵⁹*School of Physics and Astronomy, University of Edinburgh, Edinburgh, United Kingdom*

- ⁶⁰School of Physics and Astronomy, University of Glasgow, Glasgow, United Kingdom
⁶¹Oliver Lodge Laboratory, University of Liverpool, Liverpool, United Kingdom
⁶²Imperial College London, London, United Kingdom
⁶³Department of Physics and Astronomy, University of Manchester, Manchester, United Kingdom
⁶⁴Department of Physics, University of Oxford, Oxford, United Kingdom
⁶⁵Massachusetts Institute of Technology, Cambridge, MA, United States
⁶⁶University of Cincinnati, Cincinnati, OH, United States
⁶⁷University of Maryland, College Park, MD, United States
⁶⁸Los Alamos National Laboratory (LANL), Los Alamos, NM, United States
⁶⁹Syracuse University, Syracuse, NY, United States
⁷⁰Pontifícia Universidade Católica do Rio de Janeiro (PUC-Rio), Rio de Janeiro, Brazil, associated to ³
⁷¹Universidad Andres Bello, Santiago, Chile, associated to ⁵¹
⁷²School of Physics and Electronics, Hunan University, Changsha City, China, associated to ⁸
⁷³Guangdong Provincial Key Laboratory of Nuclear Science, Guangdong-Hong Kong Joint Laboratory of Quantum Matter, Institute of Quantum Matter, South China Normal University, Guangzhou, China, associated to ⁴
⁷⁴Lanzhou University, Lanzhou, China, associated to ⁵
⁷⁵School of Physics and Technology, Wuhan University, Wuhan, China, associated to ⁴
⁷⁶Henan Normal University, Xinxiang, China, associated to ⁸
⁷⁷Departamento de Física, Universidad Nacional de Colombia, Bogota, Colombia, associated to ¹⁶
⁷⁸Ruhr Universitaet Bochum, Fakultaet f. Physik und Astronomie, Bochum, Germany, associated to ¹⁹
⁷⁹Eotvos Lorand University, Budapest, Hungary, associated to ⁴⁹
⁸⁰Faculty of Physics, Vilnius University, Vilnius, Lithuania, associated to ²⁰
⁸¹Van Swinderen Institute, University of Groningen, Groningen, Netherlands, associated to ³⁸
⁸²Universiteit Maastricht, Maastricht, Netherlands, associated to ³⁸
⁸³Tadeusz Kościuszko Cracow University of Technology, Cracow, Poland, associated to ⁴¹
⁸⁴Universidade da Coruña, A Coruña, Spain, associated to ⁴⁶
⁸⁵Department of Physics and Astronomy, Uppsala University, Uppsala, Sweden, associated to ⁶⁰
⁸⁶Taras Shevchenko University of Kyiv, Faculty of Physics, Kyiv, Ukraine, associated to ¹⁴
⁸⁷University of Michigan, Ann Arbor, MI, United States, associated to ⁶⁹
⁸⁸Ohio State University, Columbus, United States, associated to ⁶⁸
- ^aUniversidade Estadual de Campinas (UNICAMP), Campinas, Brazil
^bCentro Federal de Educacão Tecnológica Celso Suckow da Fonseca, Rio De Janeiro, Brazil
^cDepartment of Physics and Astronomy, University of Victoria, Victoria, Canada
^dCenter for High Energy Physics, Tsinghua University, Beijing, China
^eHangzhou Institute for Advanced Study, UCAS, Hangzhou, China
^fLIP6, Sorbonne Université, Paris, France
^gLamarr Institute for Machine Learning and Artificial Intelligence, Dortmund, Germany
^hUniversidad Nacional Autónoma de Honduras, Tegucigalpa, Honduras
ⁱUniversità di Bari, Bari, Italy
^jUniversità di Bergamo, Bergamo, Italy
^kUniversità di Bologna, Bologna, Italy
^lUniversità di Cagliari, Cagliari, Italy
^mUniversità di Ferrara, Ferrara, Italy
ⁿUniversità di Genova, Genova, Italy
^oUniversità degli Studi di Milano, Milano, Italy
^pUniversità degli Studi di Milano-Bicocca, Milano, Italy
^qUniversità di Modena e Reggio Emilia, Modena, Italy
^rUniversità di Padova, Padova, Italy
^sUniversità di Perugia, Perugia, Italy
^tScuola Normale Superiore, Pisa, Italy
^uUniversità di Pisa, Pisa, Italy
^vUniversità della Basilicata, Potenza, Italy
^wUniversità di Roma Tor Vergata, Roma, Italy
^xUniversità di Siena, Siena, Italy
^yUniversità di Urbino, Urbino, Italy

^zUniversidad de Ingeniería y Tecnología (UTEC), Lima, Peru

^{aa}Universidad de Alcalá, Alcalá de Henares , Spain

†Deceased